Development of a Wind Turbine Rotor Flow Panel Method

A. van Garrel

ECN-E--11-071

DECEMBER 2011

Acknowledgement
Het project is uitgevoerd met subsidie van het Ministerie van Economische Zaken, Landbouw en Innovatie, regeling EOS: Lange Termijn uitgevoerd door Agentschap NL.

Project naam: ROTORFLOW-1
Contract nummer: EOSLT02016

Abstract

The ongoing trend towards larger wind turbines intensifies the demand for more physically realistic wind turbine rotor aerodynamics models that can predict the detailed transient pressure loadings on the rotor blades better than current engineering models. In this report the mathematical, numerical, and practical aspects of a new wind turbine rotor flow simulation code is described. This wind turbine simulation code is designated ROTORFLOW. In this method the fluid dynamics problem is solved through a boundary integral equation which reduces the problem to the surface of the configuration. The derivation of the integral equations is described as well as the assumptions made to arrive at them starting with the full Navier-Stokes equations. The basic numerical aspects in the solution method are described and a verification study is performed to confirm the validity of the implementation. Example simulations with the code show the flow solutions for a stationary wing and for a rotating wing in yawed conditions.

With the ROTORFLOW code developed in this project it is possible to simulate the unsteady flow around wind turbine rotors in yawed conditions and obtain detailed pressure distributions, and thus blade loadings, at the surface of the blades. General rotor blade geometries can be handled, opening the way to the detailed flow analysis of winglets, partial span flaps, swept blade tips, etc. The ROTORFLOW solver only requires a description of the rotor surface which keeps simulation preparation time short, and makes it feasible to use the solver in the design iteration process.

Contents

Nomenclature

Dimensions

$[\,l\,]$	length
$[\,m\,]$	mass
$[\,t\,]$	time

Roman symbols

g	$[\,l\,t^{-2}\,]$	gravitational acceleration
h	$[\,l\,]$	height, characteristic panel length
p	$[\,m\,l^{-1}\,t^{-2}\,]$	pressure
S	$[\,l^2\,]$	surface
V	$[\,l^3\,]$	volume
∂S	$[\,l\,]$	surface boundary
∂V	$[\,l^2\,]$	volume boundary

Greek symbols

Φ	$[\,l^2\,t^{-1}\,]$	velocity potential
φ	$[\,l^2\,t^{-1}\,]$	velocity perturbation potential
μ	$[\,l^2\,t^{-1}\,]$	dipole strength
ρ	$[\,m\,l^{-3}\,]$	mass density
σ	$[\,l\,t^{-1}\,]$	source strength

Tensors, matrices and vectors

$\vec{g}$	$[\,l\,t^{-2}\,]$	gravitational acceleration vector
$\bar{n}$	$[\,-\,]$	unit surface normal vector
$\bar{\bar{\tau}}$	$[\,m\,l^{-1}\,t^{-2}\,]$	viscous stress tensor
$\bar{\tau}$	$[\,-\,]$	unit tangential vector
$\vec{u}$	$[\,l\,t^{-1}\,]$	velocity vector
$\vec{x}$	$[\,l\,]$	coordinate vector

Subscripts, superscripts and accents

$(\ )_\infty$	onset flow value
$(\ )_n$	value in surface normal direction
$(\ )_S$	value at the surface
$(\ )^{\mathrm{T}}$	transpose operator
$(\ )_{te}$	value at the trailing edge
$(\ )_W$	value at the wake surface
$(\ )_\mu$	value from dipole singularity
$(\ )_\sigma$	value from source singularity
$(\ )^+$	value at fluid side
$(\ )^-$	value at internal side
$\vec{(\ )}$	vector
$\overline{(\ )}$	vector of unit length

1. Introduction

The ongoing trend in wind turbine design is towards larger turbines, leading to increasing investment costs and related concerns regarding risk mitigation. The increase in size also leads to relatively more flexible structures that are more susceptible to unsteady load occurrences. An important aspect of wind turbine rotor aerodynamics is the inherent unsteady character of the flow caused by variations in wind speed and direction, irregular rotational speed, blade pitch actions, rotor yaw misalignment, blade deformations and the dynamic character of the wake behind the rotor, to name a few. All this increases the need for wind turbine aerodynamics simulation tools that can predict the effects of unsteady flow on the pressure loading on the wind turbine rotor blades. The application of such a simulation tool in an engineering environment requires computation times and problem turnover times to be reasonable.

In current engineering practice the wind turbine blade loading is estimated using experimentally determined 2D airfoil characteristics for steady flow in combination with approximations for the local 'effective' onset velocity field and approximating models to compensate for unaccounted unsteady and 3D effects. This 2D approach is computationally very fast but becomes more and more questionable with increasing 3D flow and geometry characteristics. Example situations in which 3D modelling capabilities become indispensable include cases with blade rotation, blade pitch, blade sweep, rotor yaw misalignment, blade prebend, winglets, local aerodynamic control surfaces, etc.

One approach to account for the unsteady effects and the three-dimensional character of the flow problem is the deployment of solvers for the 3D unsteady Navier-Stokes equations which can in principle generate solutions for general 3D unsteady viscous flows. A drawback of this approach however is the large effort that is required to setup a simulation and the excessive computational time to obtain a solution.

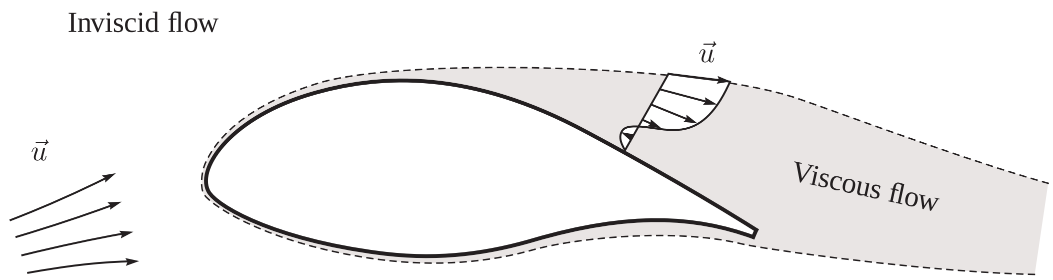

Figure 1.1: Domain decomposition into an inviscid flow region and a viscous flow region.

The approach taken here is to combine the advantages of above two approaches and develop a solution method capable of providing detailed unsteady 3D wind turbine rotor flow solutions while avoiding excessive computational costs. To this end the flow domain is decomposed into two subdomains: an outer region in which the flow is considered incompressible and inviscid and is formulated in terms of a potential flow solver, and an inner region where the effects of viscosity will be taken into account by an integral boundary layer solver (see Van Garrel [8]) as sketched in Figure 1.1. The two domains will be coupled through a so-called viscous-inviscid interaction procedure. Both the development of the boundary layer solver (Özdemir and Van den Boogaard [13]) and the viscous-inviscid interaction procedure (Bijleveld and Veldman [4]) are currently underway at ECN.

In this report the development of the potential flow solver for incompressible, inviscid 3D flows is discussed. The code under development will be referred to as ROTORFLOW.

The mathematical theory that forms the basis of flow field description for the incompressible inviscid flow in the outer region of the ROTORFLOW code is described in Chapter 2.

In Chapter 3 some specific topics in the discretization of the mathematical model will be discussed.

Some basic verification tests are reported in Chapter 4 for two grid types of a tri-axial ellipsoid and the order of convergence will be established for this geometry.

Finally, in Chapter 5 some applications of the ROTORFLOW code for lifting bodies are shown.

2. Potential Flow Model

The mathematical model for the three-dimensional unsteady flow around wind turbine rotors is considered. The flow is assumed to be incompressible and the effects of viscosity are assumed to be confined to thin boundary layer and wake regions due to the high operational Reynolds numbers. Outside these regions the flow is assumed to be irrotational. The effects of heat conduction are considered negligible. The main area of interest lies in the detailed prediction of the unsteady pressure loading on the wind turbine rotor blades as occurring during normal operation. An accurate representation of the wake behind the rotor is of interest for its influence on the flowfield around the upstream rotor blades.

Above observations and assumptions make it justifiable to model the flow around wind turbine rotors with the fluid dynamics equations for unsteady potential flow. These equations will be cast in a boundary integral equation form.

2.1. Introduction

A continuously differentiable flowfield around an arbitrary body in 3D space can be described in terms of velocity vector $\vec{u}(\vec{x})$ or equivalently in terms of source $\sigma(\vec{x})$ and vorticity $\vec{\omega}(\vec{x})$ distributions throughout the volume plus an irrotational and solenoidal onset flow $\vec{u}_\infty(\vec{x})$ as depicted in Figure 2.1.

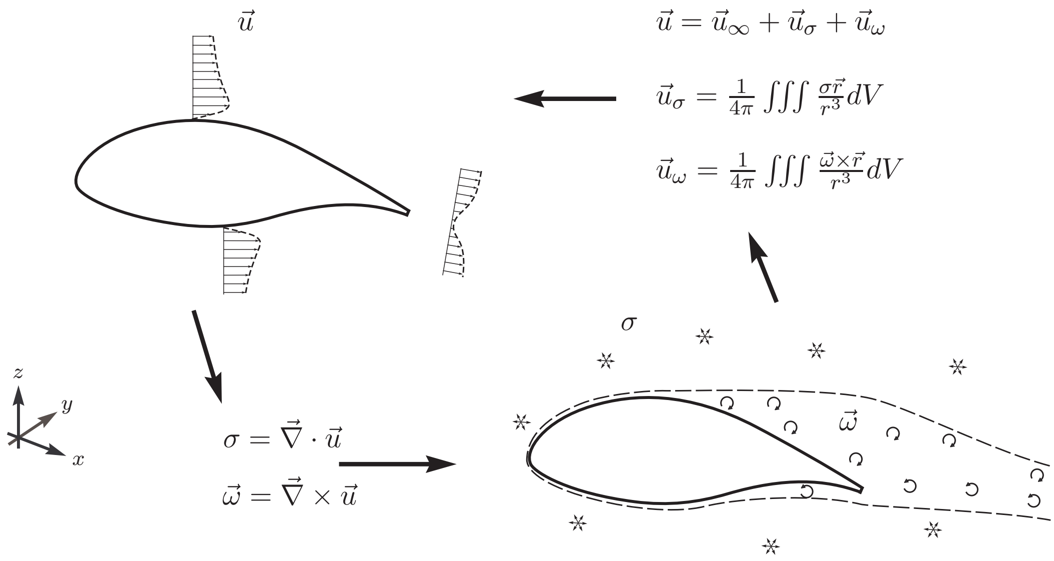

Figure 2.1: Flowfield representation in terms of velocity vector field $\vec{u}(\vec{x})$ or in terms of sources $\sigma(\vec{x})$ and vortices $\omega(\vec{x})$.

An approximation to the volumetric source and vorticity distributions is to restrict them to the body and wake surfaces as indicated in Figure 2.2 which will lead to divergence free and irrotational flow everywhere except across these surfaces. The resulting boundary integral equations can be solved with a so called panel method in which the surface of the configuration is covered with panels where boundary conditions are imposed in selected points.

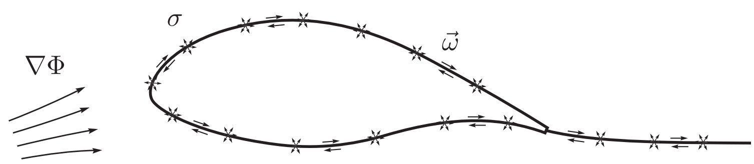

Figure 2.2: Flowfield approximation.

2.2. Governing Equations

General fluid flows are described by the Navier-Stokes equations that express the physical principles of conservation of mass, momentum, and energy. For a point $\vec{x}$ in volume $V \in \mathbb{R}^3$ at time t, the equations for mass, momentum, and energy conservation in differential form are respectively

$$\frac{\partial \rho}{\partial t} + \nabla \cdot (\rho \vec{u}) = 0, \tag{2.1}$$

$$\frac{\partial (\rho \vec{u})}{\partial t} + \nabla \cdot (\rho \vec{u} \vec{u}) + \nabla p - \rho \vec{g} - \nabla \cdot \bar{\bar{\tau}} = \vec{0}, \tag{2.2}$$

$$\frac{\partial (\rho E)}{\partial t} + \nabla \cdot (\rho E \vec{u}) + \nabla \cdot (p \vec{u}) - \rho \vec{g} \cdot \vec{u} - \dot{Q} + \nabla \cdot \vec{q} - \nabla \cdot (\bar{\bar{\tau}} \cdot \vec{u}) = 0, \tag{2.3}$$

with $\rho(\vec{x}, t)$ the mass density, $\vec{u}(\vec{x}, t)$ the fluid velocity, pressure $p(\vec{x}, t)$, $\vec{g}$ the gravitational acceleration vector, and $\bar{\bar{\tau}}(\vec{x}, t)$ the viscous stress tensor. The total energy per unit mass is denoted by $E(\vec{x}, t)$ and the term $\dot{Q}(\vec{x}, t)$ in the energy equation (2.3) is the heating that works on the fluid volume directly, for example by radiation, and has dimension 'energy per unit volume per unit time'. Heating due to thermal conduction is accounted fort by the term with heat flux vector $\vec{q}(\vec{x}, t)$ that has dimension 'energy per unit area per unit time'.

To close the system of equations, the Navier-Stokes equations are supplemented by two equations of state and two constitutive relations. The latter model the viscous stress tensor $\bar{\bar{\tau}}(\vec{x}, t)$ and the heat flux vector $\vec{q}(\vec{x}, t)$ in terms of available variables. See Appendix B for more details.

We consider the fluid dynamics equations for wind turbine applications where the flow is assumed to be incompressible and the effects of heating are considered negligible. Fluid particle mass density is considered constant. The effects of viscosity are assumed to be negligible due to the high operational Reynolds numbers. These considerations make it feasible to reduce the set of equations. For unsteady incompressible flow, the mass conservation equation reduces to

$$\nabla \cdot \vec{u} = 0. \tag{2.4}$$

Note that although the equation does not have an explicit time derivative term, unsteady boundary conditions will introduce time dependency in the solution. The equations expressing momentum conservation for unsteady, incompressible, inviscid flows read:

$$\rho \frac{\partial \vec{u}}{\partial t} + \rho (\vec{u} \cdot \nabla) \vec{u} + \nabla (p + \rho g h) = \vec{0}, \tag{2.5}$$

where h is the distance above the ground.

A significant reduction in complexity can be achieved if it is assumed that rotational flow is confined to infinitesimal thin boundary layer and wake regions, an is irrotational everywhere else, that is $\nabla \times \vec{u} = \vec{0}$. This allows us to write the velocity vector field $\vec{u}(\vec{x}, t)$ as the gradient of a scalar velocity potential function $\Phi(\vec{x}, t)$:

$$\vec{u} = \nabla \Phi. \tag{2.6}$$

Substitution of the velocity potential gradient (2.6) in the continuity equation (2.4) gives the Laplace equation for the velocity potential in domain V:

$$\nabla\cdot\nabla\Phi = 0. \tag{2.7}$$

Substituting the gradient of the velocity potential (2.6) in the momentum conservation equations (2.5) results in the Bernoulli equation for unsteady potential flow:

$$\frac{\partial\Phi}{\partial t} + \frac{1}{2}\nabla\Phi\cdot\nabla\Phi + \frac{p}{\rho} + gh = C(t). \tag{2.8}$$

2.3. Boundary Integral Equation

It is assumed that flow domain domain V can be decomposed into a set of non-overlapping volumes V_m with boundaries ∂V_m (see Figure 2.3). Let $S_{m,k}$ be the part of the boundary that the two volumes V_m and V_k have in common:

$$S_{m,k} = \partial V_m \cap \partial V_k, \qquad m \neq k.$$

The surface S of the configuration and its wake is now described by the complete set of inner boundaries:

$$S = \cup S_{m,k}.$$

It can be shown (Appendix C) that the solution of the Laplace equation (2.7) for the velocity potential $\Phi(\vec{x}_P, t)$ in a point $\vec{x}_P$ in volume V can be formulated in terms of a reference velocity potential $\Phi_\infty(\vec{x}_P, t)$ and perturbation velocity potential contributions $\varphi_\mu(\vec{x}_P, t)$ and $\varphi_\sigma(\vec{x}_P, t)$ from dipole singularity distributions $\mu(\vec{x}_Q, t)$ and source singularity distributions $\sigma(\vec{x}_Q, t)$ on the inner boundaries repectively, that is

$$\Phi \;=\; \Phi_\infty \;+\; \varphi_\mu \;+\; \varphi_\sigma, \tag{2.9}$$

where $\Phi_\infty(\vec{x}_P, t)$ is the unperturbed velocity potential in point $\vec{x}_P$, the velocity potential if no inner boundaries were present. However, the unperturbed velocity potential Φ_∞ could also include contributions from a designated set of source and dipole singularities in the nearby flow field.

The perturbation velocity potentials induced in point $\vec{x}_P$ by the dipole and source distributions on surface S are defined by

$$\varphi_\mu(\vec{x}_P, t) = \frac{-1}{4\pi}\iint\limits_S \mu\,\frac{\bar{n}_m\cdot\vec{r}}{r^3}\,dS, \tag{2.10}$$

$$\varphi_\sigma(\vec{x}_P, t) = \frac{-1}{4\pi}\iint\limits_S \sigma\,\frac{1}{r}\,dS, \tag{2.11}$$

where $\bar{n}_m(\vec{x}_Q, t)$ is the unit normal vector in $\vec{x}_Q \in \partial V_{m,k}$ that is pointing into volume V_m. The vector $\vec{r}$ is defined as the vector from a point $\vec{x}_Q$ on the surface to evaluation point $\vec{x}_P$, whereas its length is denoted by r, that is,

$$\vec{r} = \vec{x}_P - \vec{x}_Q, \quad r = |\vec{r}\,|, \qquad \text{for} \quad \vec{x}_Q \in S_{m,k}. \tag{2.12}$$

For problems where the evaluation point $\vec{x}_P$ and the boundary $S_{m,k}$ are moving relative to each other, we have $\vec{r} = \vec{r}(t)$.

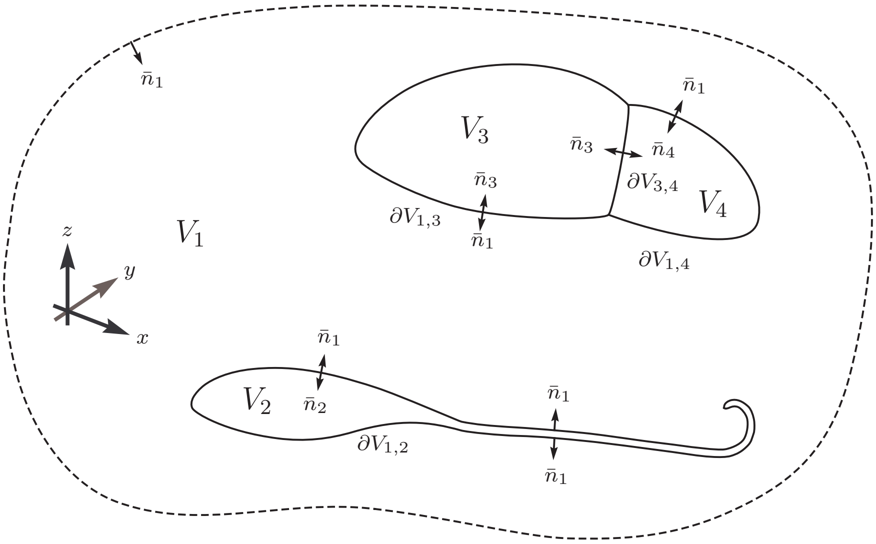

Figure 2.3: The flow domain $V \in \mathbb{R}^3$ is the union of the non-overlapping volumes V and inner boundaries $\partial V_{m,k}$ that separate volume V_m from volume V_k. Unit normal vector $\bar{n}_m$ is defined to point into volume V_m.

The dipole strength $\mu(\vec{x}_Q, t)$ and the source strength $\sigma(\vec{x}_Q, t)$ in point $\vec{x}_Q$ at the surface, are related to the velocity potential values $\Phi_m(\vec{x}_Q, t)$ and $\Phi_k(\vec{x}_Q, t)$ on both sides of the surface by

$$\mu(\vec{x}_Q, t) = -(\Phi_m - \Phi_k), \tag{2.13}$$

$$\sigma(\vec{x}_Q, t) = \nabla(\Phi_m - \Phi_k) \cdot \bar{n}_m. \tag{2.14}$$

As shown in Appendix C, the integral for the dipole singularity distribution causes a jump in the velocity potential of strength $\mu(\vec{x}_P, t)$ across the surface:

$$\varphi(\vec{x}_P \to S^{\pm}, t) \;=\; \varphi^p_\sigma(\vec{x}_P, t) + \varphi^p_\mu(\vec{x}_P, t) \;\mp\; \frac{1}{2}\,\mu(\vec{x}_P, t), \tag{2.15}$$

where S^+ and S^- denote the sides of $S_{m,k}$ when approached from volume V_m or from volume V_k respectively. The two $\varphi^p(\vec{x}_P \in S)$ terms on the right hand side of equation (2.15) are to be interpreted as Cauchy Principal Value or Finite Part integrals over the complete set of inner surfaces, with an infinitesimal region around the singular point excluded from the surface of integration.

2.4. Boundary Conditions

The goal is now to find a solution for the Laplace equation (2.7) for the potential field $\Phi(\vec{x}_P, t)$ as formulated in terms of reference potential field $\Phi_\infty(\vec{x}_P, t)$ plus source and dipole perturbation potential fields $\varphi_\sigma(\vec{x}_P, t)$ and $\varphi_\mu(\vec{x}_P, t)$, subject to the appropriate boundary conditions.

For surfaces of thick bodies we will employ internal Dirichlet boundary conditions as introduced by Morino and Kuo [12]. This formulation assumes that we are only interested in the flow field on one side of the surface, and that the volume at the other side of the surface is of no interest and can be prescribed. This excludes the use of internal Dirichlet boundary conditions for the flow over infinitesimal thin surfaces.

2.4.1. Body Surface

For thick bodies, the internal Dirichlet formulation will be employed where it is assumed that only the solution in the volume on one side of the surface is of interest. Let S^+ denote the side of surface $S_{m,k}$ in volume V_m where we want to obtain a solution of the flow problem, and let S^- denote the side of the surface $S_{m,k}$ in volume V_k that is considered non-physical and exhibits a fictitious flow.

The boundary condition at surface side S^+ is such that the flow velocity at the surface in normal direction, is equal to normal component of the surface velocity $\vec{u}_S(\vec{x}_P, t)$, plus a specified velocity $v_n(\vec{x}_P, t)$ in normal direction:

$$\nabla\Phi_m \cdot \bar{n}_m \;=\; \vec{u}_S \cdot \bar{n}_m \;+\; v_n, \qquad \vec{x}_P \to S^+. \tag{2.16}$$

The normal velocity distribution can be used for example to simulate boundary layer displacement thickness effects or for the simulation of inflow through a suction slot. The local surface velocity $\vec{u}_S(\vec{x}_P, t)$ may be composed of solid body rotation, surface translation, surface rate of deformation and so on.

Suppose the velocity potential in the fictitious flow domains V_k is known in advance,

$$\Phi_k = \Phi_k(\vec{x}_P, t), \qquad \vec{x}_P \in V_k, \tag{2.17}$$

and let

$$\vec{u}_k(\vec{x}_P, t) = \nabla\Phi_k, \qquad \vec{x}_P \in V_k. \tag{2.18}$$

For point $\vec{x}_P$ in region V_k approaching the surface S^-, the boundary integral equation (2.9) now reads:

$$\varphi_\mu(\vec{x}_P, t) \;+\; \varphi_\sigma(\vec{x}_P, t) \;=\; \Phi_k(\vec{x}_P, t) - \Phi_\infty(\vec{x}_P, t), \qquad \vec{x}_P \to S^-. \tag{2.19}$$

Substitution of the boundary condition (2.16) at S^+ and the known velocity potential in volume V_k (2.17) in the definition of the source strength (2.14), gives an expression for the source strength in terms of known quantities:

$$\sigma(\vec{x}_Q, t) = (\vec{u}_S \;-\; \vec{u}_k) \cdot \bar{n}_m \;+\; v_n, \qquad \vec{x}_Q \in S. \tag{2.20}$$

The boundary integral equation (2.19) at $\vec{x}_P \to S^-$ now gives an expression involving the unknown dipole strength $\mu(\vec{x}_Q, t)$ as a function of known quantities.

Taking the surface gradient of the dipole strength (2.13) gives us for the tangential component of the velocity at the surface side of interest S^+

$$\nabla_S\Phi_m(\vec{x}_P, t) \;=\; \nabla_S\Phi_k \;-\; \nabla_S\mu, \qquad \vec{x}_P \to S^+. \tag{2.21}$$

Combining the normal velocity from the boundary condition (2.16), the expression for the source strength in equation (2.20), and the tangential velocity from equation (2.21) gives an expression for the velocity at the surface in the inertial coordinate system:

$$\vec{u}(\vec{x}_P, t) \;=\; \vec{u}_k \;+\; \sigma\,\bar{n}_m \;-\; \nabla_S\mu, \qquad \vec{x}_P \to S^+. \tag{2.22}$$

Equation (2.22) states that the velocity at the surface side of interest is composed of a known base flowfield $\vec{u}_k$ and a perturbation flowfield due to the source and dipole singularity distributions.

Notice that the velocity potential field Φ_k, and consequently velocity field $\vec{u}_k$, still has to be defined in the non-physical domains. This gives some freedom to base this choice on the properties that the resulting set of equations will have. A choice that is expected to give small numerical errors is one that results in smooth and weak source and dipole distributions. Here it is decided to set the fictitious flowfield equal to the onset flowfield as was introduced by Morino and Kuo [12], that is $\Phi_k = \Phi_\infty$, and $\vec{u}_k = \vec{u}_\infty$. Assuming a known surface velocity $\vec{u}_S$ and normal velocity v_n, this gives the following set of equations to determine the velocity distribution at the surface:

$$\begin{array}{lcll} \sigma & = & (\vec{u}_S - \vec{u}_\infty)\cdot\bar{n} + v_n\bar{n}, & \\ \varphi_\mu & = & -\varphi_\sigma, & \vec{x}_P \to S^-, \\ \vec{u}(\vec{x}_P,t) & = & \vec{u}_\infty \,+\, \sigma\,\bar{n} \,-\, \nabla_S\mu, & \vec{x}_P \to S^+. \end{array} \tag{2.23}$$

2.4.2. Wake Surface

In the previous section we derived a set of equations to determine the dipole strength distribution the solid body surface. In this section the conditions for the wake surface will be determined. At the trailing edge of a lifting body, the point where the vorticity leaves the surface (see Figures 2.1 and 2.2), a linear Kutta condition will be imposed that results in a smooth flow with finite velocity at that point. This condition was used by Morino and Kuo [12] and equates the dipole strength at the start of the wake equal to the jump in dipole strengths across the trailing edge:

$$\mu_{w_{te}} = [\![\varphi]\!]_{te} = [\![\mu]\!]_{te}. \tag{2.24}$$

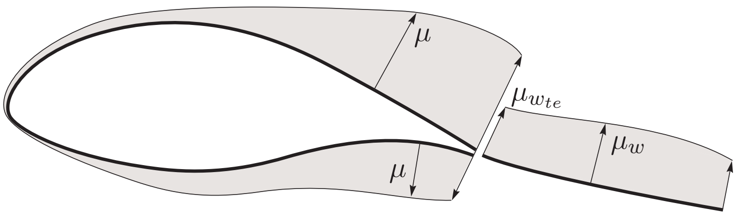

Figure 2.4: Trailing edge Kutta condition.

For the evolution of the wake we will make use of the theorems of Helmholtz and Kelvin for vorticity dynamics (see Batchelor [3], Cottet and Koumoutsakos [5], Saffman [14]). In incompressible flows the inviscid evolution of the vorticity field can be obtained by applying the curl operator to the momentum conservation equation 2.2. After some manipulation, the resulting Lagrangian description is

$$\frac{\mathrm{D}\vec{\omega}}{\mathrm{D}t} = \vec{\omega}\cdot\nabla\vec{u}. \tag{2.25}$$

A similar relationship is valid for material line elements $\delta\vec{l}$ and can be obtained by replacing $\vec{\omega}$ in above equation with $\delta\vec{l}$. We can thus conclude that in incompressible inviscid flows, vortex lines behave as material line elements. Kelvin's circulation theorem for incompressible inviscid flows reads

$$\frac{\mathrm{D}\Gamma}{\mathrm{D}t} = 0, \tag{2.26}$$

where circulation Γ is defined by a surface integral of vorticity over a cross section of a vortex tube or recast into a contour integral around the vortex tube with the help of Stokes' theorem (see Appendix A)

$$\Gamma = \iint\limits_S \vec{\omega}\cdot\bar{n}\;dS \;=\; \int\limits_{\partial S} \vec{u}\cdot\bar{\tau}\;ds, \tag{2.27}$$

with $\bar{n}$ the unit normal vector to the cross section surface S, and $\bar{\tau}$ the unit vector tangential to the contour ∂S. From above equations it can be concluded that in incompressible inviscid flows a tube of vorticity preserves its identity when moving with the fluid. In terms of the evolution of wake element position $\vec{X}_w$ and wake element dipole strength μ_w the corresponding equations are

$$\frac{\mathrm{d}\vec{X}_w}{\mathrm{d}t} = \vec{u}, \qquad \vec{X}_\mu(t_0) = \vec{x}_{te}(t_0), \tag{2.28}$$

and

$$\frac{\mathrm{D}\mu_w}{\mathrm{D}t} = 0, \qquad \mu_w(t_0) = \mu_{w_{te}}(t_0), \tag{2.29}$$

where t_0 is the time of wake element creation.

2.5. Aerodynamic Forces

The total force and moment with respect to the coordinate system origin are determined by integrating the pressure force over the surface of the configuration (see Figure 2.5):

$$\vec{F}(t) = \iint\limits_S p\,\bar{n}\;dS, \tag{2.30}$$

$$\vec{M}(t) = -\iint\limits_S p\,\bar{n} \times \vec{r}\;dS, \tag{2.31}$$

where $\vec{r}$ is the position vector to the surface, and p the pressure that can be obtained from the Bernoulli equation (2.8).

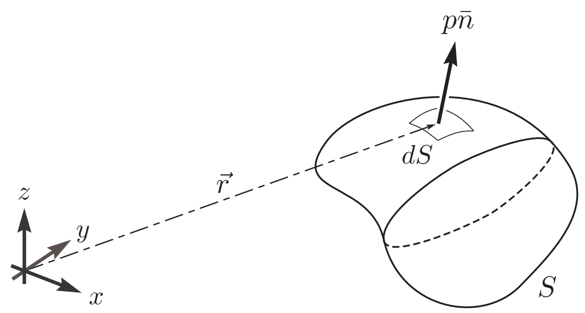

Figure 2.5: Infinitesimal surface contribution to the total force and moment acting on the configuration.

3. Numerical Approach

The continuous mathematical description of the flow problem for wind turbine applications will be discretized such that it is possible to numerically determine the solution with a *panel method*. To this end we will introduce approximations and discretizations for the geometry, the singular surface integral equations, and the boundary conditions. The geometry will be described in terms of bodies and wakes that consist of patches of structured grid cells, the so called 'panels' in the method. The quadrilateral panels will be described by a bilinear geometry where possible and by a planar surface elsewhere. Each panel on a body or wake patch is assigned a constant strength dipole distribution and for body patches the panels are also assigned a constant strength source distribution. Just below the surface of the body panel midpoints so called *collocation points* are located where the boundary conditions will be fulfilled.

3.1. Geometry

The surface of the configuration is subdivided into one or more patches which are discretized in a structured grid fashion. The grid cells on the surface of the configuration are in the boundary integral discretization called 'panels', hence the name panel method for this type of solution method. An example rotor blade surface subdivided into multiple patches, each patch consisting of an array of panels, is shown in Figure 3.1.

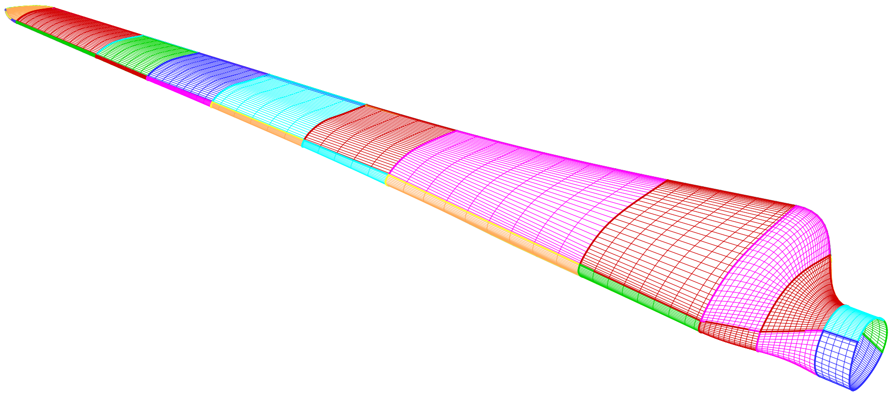

Figure 3.1: Rotor blade surface subdvided into multiple patches.

Each patch consist of an array of nodes in i and j direction (see Figure 3.2b) which determine the corner nodes of the panels. The vector normal to the surface is defined to be in the direction of the right-hand cross product $\bar{n} \equiv \bar{i} \times \bar{j}$ as is indicated in Figure 3.2a.

3.2. Panel Method

The boundary integral equations in (2.23) are discretized as a low-order panel method (see Hoeijmakers [9], Katz and Plotkin [10]). In this approach each panel carries a constant strength source σ and/or dipole μ singularity distribution. Boundary conditions are enforced in each panel col-

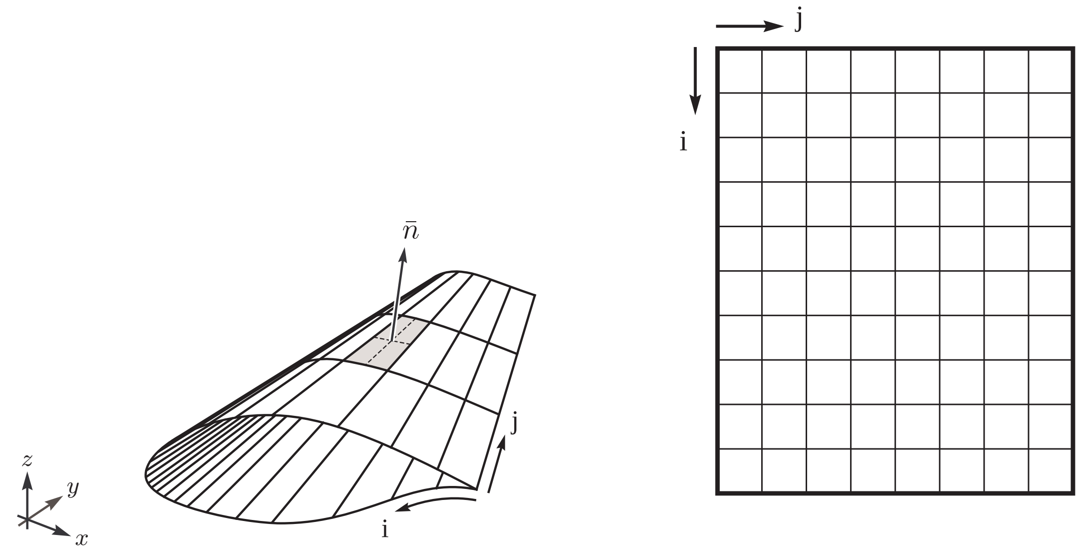

(a) The normal vector $\bar{n}$ is assumed to point into the flow domain and is deduced from the right-hand vector cross product of the i and j directions: $\bar{n} \equiv \bar{i} \times \bar{j}$

(b) Patch node and panel ordering in a structured grid using i and j directions. Here the normal vector points out of the paper.

Figure 3.2: Node ordering and panel normal vectors in a patch.

location point $\vec{x}_i$, located just below the panel's surface midpoint. The resulting set of discrete equations for the $i = 1..N$ collocation points is

$$\sum_j A_{ij}\mu_j + \sum_j B_{ij}\sigma_j = 0, \qquad \text{for} \quad i = 1..N, \tag{3.1}$$

where A_{ij} and B_{ij} are so-called aerodynamic influence coefficients defined by

$$A_{ij} = \frac{-1}{4\pi} \iint_{S_j} \frac{\bar{n}_j \cdot \vec{r}}{r^3}\, dS, \tag{3.2}$$

$$B_{ij} = \frac{-1}{4\pi} \iint_{S_j} \frac{1}{r}\, dS, \tag{3.3}$$

in which

$$\vec{r} = \vec{x}_i - \vec{x}_Q, \quad r = |\vec{r}|, \quad \text{and} \quad \vec{x}_Q \in S_j. \tag{3.4}$$

3.2.1. Dipole Velocity Potential

The velocity potential induced at point $\vec{x}_P$ by a panel with surface S_j and dipole distribution μ is given by

$$\varphi_\mu(\vec{x}_P) = \frac{-1}{4\pi} \iint_{S_j} \mu \frac{\bar{n} \cdot \vec{r}}{r^3}\, dS, \tag{3.5}$$

where

$$\vec{r} = \vec{x}_P - \vec{x}_Q, \quad r = |\vec{r}|, \quad \text{and} \quad \vec{x}_Q \in S_j. \tag{3.6}$$

The usual approach taken in low-order panel methods is to use a flat approximation for the panel geometry for which analytical results exists for the integral in equation (3.5) (see Katz and

Plotkin [10]). Flat panels, however, lead to gaps between the panels in the surface approximation, that grow larger with increasing surface twist. Especially for panels in a highly deformed wake surface this flat panel approximation is inadequate. The approach taken here is to use a bilinear representation for the panel geometry (see Figure 3.3) which gives a better surface approximation and avoids gaps altogether.

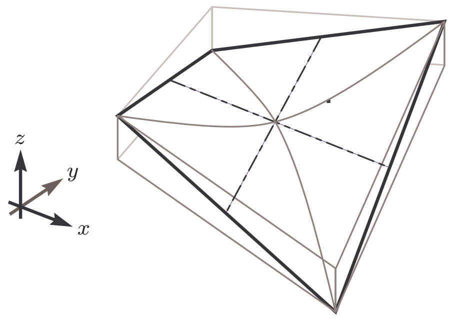

Figure 3.3: A bilinear quadrilateral panel.

For a unit strength dipole distribution ($\mu = 1$) the integral in equation (3.5) is equal to the solid angle and can be determined by the projection of the warped panel on a sphere with unit radius and the evaluation point $\vec{x}_P$ as its center (see Figure 3.4). The solid angle is then the ratio between the projected panel area and the surface area of the sphere. We use the fact that the area of a quadrilateral on a sphere with unit radius is equal to the sum of the included angles minus 2π:

$$\text{area} = -2\pi + \sum_{i=1}^{4} \beta_i. \tag{3.7}$$

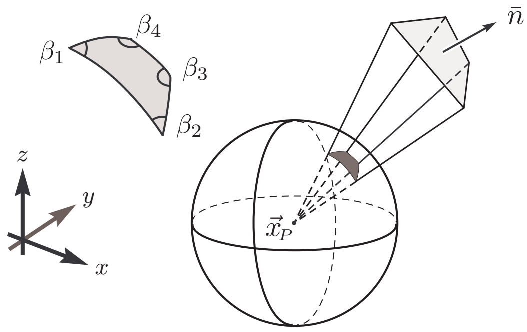

Figure 3.4: The solid angle is the ratio between the area of the projected panel and the surface area of the sphere with the evaluation point as its center. The area of the projected quadrilateral can be determined from its included angles β_i.

3.2.2. Source Velocity Potential

The velocity potential induced by a panel with surface S_j and source distribution σ in point $\vec{x}_P$ is given by

$$\varphi_\sigma(\vec{x}_P) = \frac{-1}{4\pi} \iint_{S_j} \sigma \frac{1}{r} \, dS. \tag{3.8}$$

For the exact evaluation of this integral for constant source strength σ on each panel the reader is referred to the analytical formula in Katz and Plotkin [10].

3.2.3. Dipole Surface Gradient Velocity

To obtain the total velocity $\vec{u}$ at the boundary of the configuration, one of the components in equation (2.22) that has to be determined is the surface gradient of the dipole strength $\nabla_S \mu$. This is accomplished with the help of with Gauß' Theorem (see Appendix A), giving an expression for the average dipole surface gradient inside contour ∂S (see Figure 3.5):

$$\overline{\nabla_S \mu} = \frac{1}{S} \int\limits_{\partial S} \mu \, \bar{\nu} \, ds, \tag{3.9}$$

where $\bar{\nu}$ is the unit outward vector normal to the contour and tangential to the surface. The contour ∂S is defined by the collocation points of four neighboring panel. As an approximation, the perturbation velocity in the grid node due to the dipole distribution is assigned this average surface gradient.

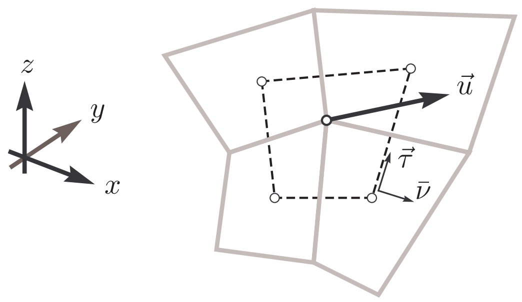

Figure 3.5: Definitions used in the contour integral to determine the surface perturbation velocity in a grid node due to a dipole distribution.

4. Verification

In this chapter the results of the convergence tests on an ellipsoid with semi-axes $4, 2, 1$ are reported. For tri-axial ellipsoids analytical solutions exist. This makes it possible to verify the implemented panel method for correctness of system of equation setup, the solution of the system by a linear equation solver, and the application of postprocessing steps necessary to obtain the surface velocity distribution. The verification tests are performed for a single patch grid that exhibits two grid poles, and a six patch grid that does not possess collapsed edges. It is shown that for the tri-axial ellipsoid the rate of convergence for the perturbation potential and the pressure coefficient surface distributions are up to order $\mathcal{O}(h^2)$, where h is a characteristic panel length.

4.1. Analytical Solution

For ellipsoidal bodies in potential flow analytical solutions exist (see Durand [1], Lamb [11]). If we define the function $\psi(\vec{x})$ as

$$\psi(\vec{x}) = \left(\frac{x}{a}\right)^2 + \left(\frac{y}{b}\right)^2 + \left(\frac{z}{c}\right)^2 - 1, \tag{4.1}$$

the surface of an ellipsoid with semi-axes a, b, c is described by $\psi(\vec{x}_e) = 0$. The perturbation potential on the surface of this ellipsoid for a general onset flow $\vec{u}_\infty = (u_\infty, v_\infty, w_\infty)^{\mathrm{T}}$, is given by

$$\varphi(\vec{x}_e) = u_\infty x_e \frac{\alpha_0}{2-\alpha_0} + v_\infty y_e \frac{\beta_0}{2-\beta_0} + w_\infty z_e \frac{\gamma_0}{2-\gamma_0}, \tag{4.2}$$

where

$$\alpha_0 = \int_0^\infty \frac{a\,b\,c}{(a^2+\lambda)\sqrt{(a^2+\lambda)(b^2+\lambda)(c^2+\lambda)}}\,d\lambda, \tag{4.3}$$

$$\beta_0 = \int_0^\infty \frac{a\,b\,c}{(b^2+\lambda)\sqrt{(a^2+\lambda)(b^2+\lambda)(c^2+\lambda)}}\,d\lambda, \tag{4.4}$$

$$\gamma_0 = \int_0^\infty \frac{a\,b\,c}{(c^2+\lambda)\sqrt{(a^2+\lambda)(b^2+\lambda)(c^2+\lambda)}}\,d\lambda. \tag{4.5}$$

Above integrals are regular and can be numerically evaluated given a specific choice for semi-axes a, b, c. In the current study, the integrals were integrated with an adaptive Simpson's quadrature rule. For the total potential on the surface of the ellipsoid we can write

$$\Phi(\vec{x}_e) \;=\; \vec{u}_\infty \cdot \vec{x}_e + \varphi(\vec{x}_e) \;=\; \frac{2u_\infty}{2-\alpha_0} x_e + \frac{2v_\infty}{2-\beta_0} y_e + \frac{2w_\infty}{2-\gamma_0} z_e. \tag{4.6}$$

The velocity vector on the surface of the ellipsoid can now be determined from the surface gradient of the total potential (4.6).

4.2. Geometric Convergence

First the convergence of the discretised geometry towards the exact ellipsoidal surface is investigated. The investigated geometric norm is based on the distance between the panel mid points $\vec{x}_c$, and the points $\vec{x}_e$ on the surface of the ellipsoid. The surface is discretized as a single-domain grid with poles along the x-axis as shown in Figure 4.2a. The vertex coordinates are obtained by scaling a sphere with a cosine distribution in x-direction and an equidistant distribution in circumferential direction. An $m \times m$ panelling was used for the geometric convergence study, with $m = 8, 16, 32, \dots, 1024$. The points $\vec{x}_e$ are obtained by projecting the collocation points $\vec{x}_c$ along the normal vector $\bar{n}_c$ onto the surface.

The discrete versions of the error norms are defined by

$$\mathrm{L}_1(x) = \frac{1}{n}\sum_{i=1}^{n} |x_i|, \tag{4.7}$$

$$\mathrm{L}_2(x) = \left(\frac{1}{n}\sum_{i=1}^{n} |x_i|^2\right)^{1/2}, \tag{4.8}$$

$$\mathrm{L}_\infty(x) = \max_{i=1,n} |x_i|, \tag{4.9}$$

where $|x_i|$ is the absolute value of the difference between exact and approximated values in case of scalar quantities, and the length of the vector differences in case of vectorial quantities.

The variation of the error norms with h^{-1} is shown in Figure 4.1, where $h = N^{-\frac{1}{2}}$ is a characteristic panel length and N the total number of panels. As can be seen, the error is $\mathcal{O}(h^2)$ in the geometric norms as expected. It should be noted that the largest errors were invariably for panels near the poles in the grid. This gives an indication that for practical purposes we would have to refine the mesh in these regions of large surface curvature to obtain a more evenly distributed error.

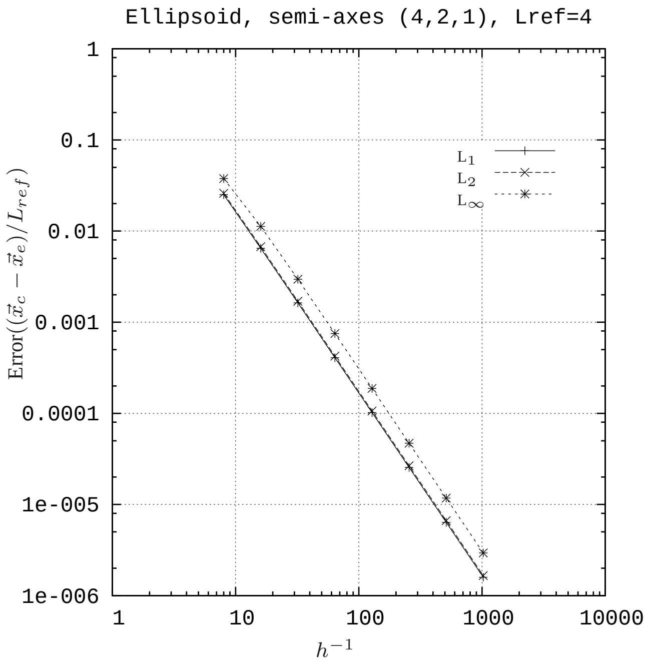

Figure 4.1: Geometric convergence of distance between panel mid points and the surface of an ellipsoid with semi-axes $4, 2, 1$ as a function of h^{-1}, where h is a characteristic panel length.

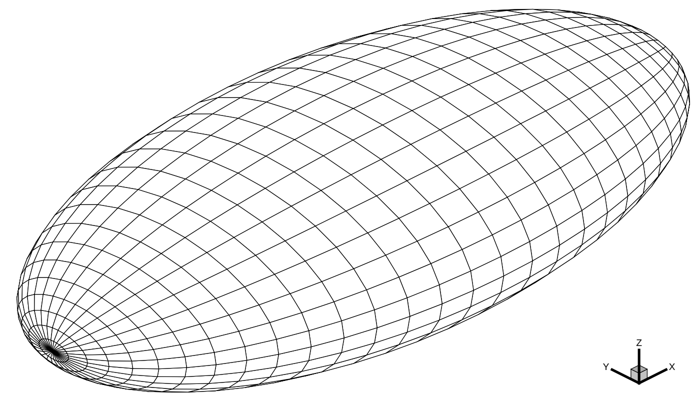

(a) Single patch, 32×32 panelling.

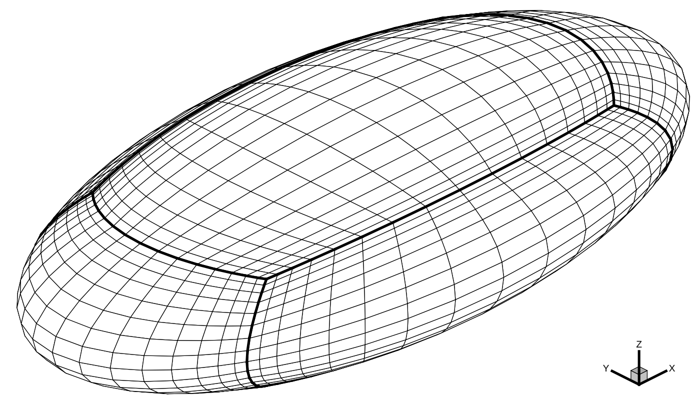

(b) Six patches, $16 \times 16 \times 16$ panelling.

Figure 4.2: Panellings for a spheroid with semi-axes $4, 2, 1$.

4.3. Velocity Potential Convergence

In the panel method that is implemented, the perturbation potential in the collocation points of the panels is obtained using a direct solver for the system of equations. The perturbation potential thus obtained, is compared to the analytical solution in the points projected in normal direction at the exact ellipsoid surface. For this study two panellings are used, a single patch panelling and a six patch panelling, of which example grids are shown in Figure 4.2. The six patch ellipsoid was introduced to see if the behaviour in the grid poles of the single patch configuration could be avoided.

4.3.1. Single Patch Grid

In Figure 4.3, the error in the velocity potential is shown as a function of characteristic panel length h for the single patch grid. As can be seen, the error is of $\mathcal{O}(h^2)$ in the velocity potential for this panelling. The largest errors appear near the poles of the grid, which in this case coincide with the areas of largest surface curvature, as is shown in Figures 4.4 and 4.5. In case the stagnation points coincide with the poles of the grid, the largest errors occurs elsewhere on the surface as can be seen in Figure 4.6.

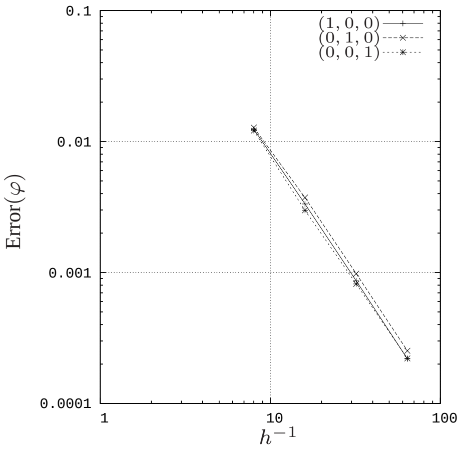

(a) L_1-norms.

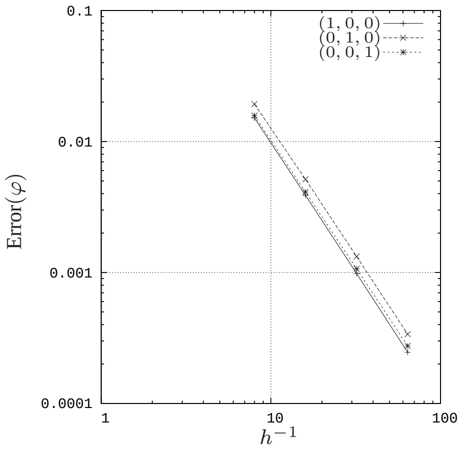

(b) L_2-norms.

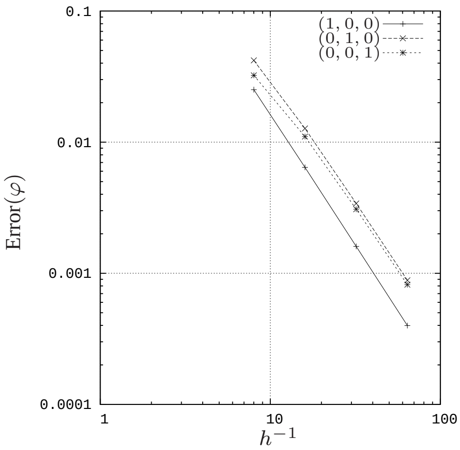

(c) L_∞-norms.

Figure 4.3: Error norms in perturbation potential as a function of h^{-1}, where h is a characteristic panel length, for onset flows along the three coordinate axes of a single patch grid.

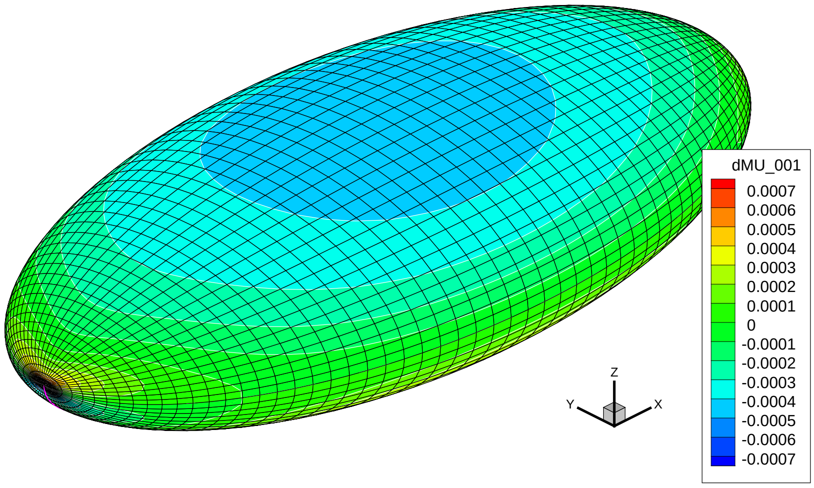

(a) Perturbation potential error.

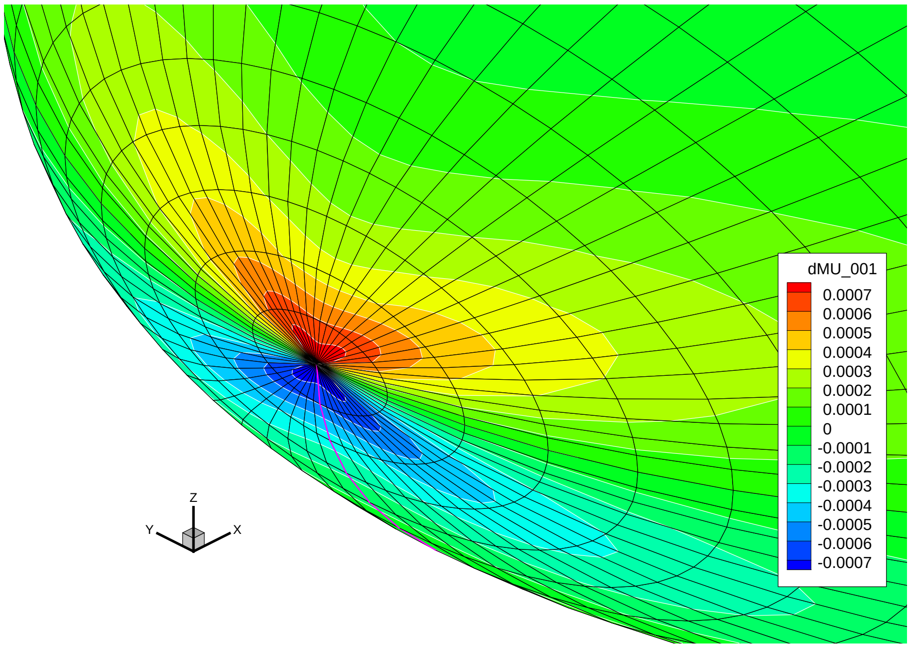

(b) Closeup of the pole region.

Figure 4.4: Perturbation potential error distribution for a single patch 64×64 panel ellipsoid and an onset flow in z-direction. The largest errors appear near the poles of the grid.

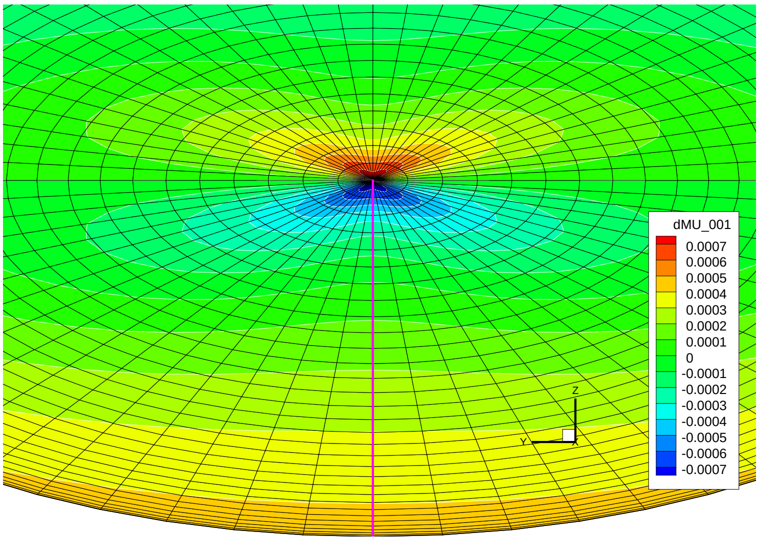

Figure 4.5: Perturbation potential error distribution for a single patch 64×64 panel ellipsoid and an onset flow in z-direction. A smooth potential error distribution across the patch edges is shown.

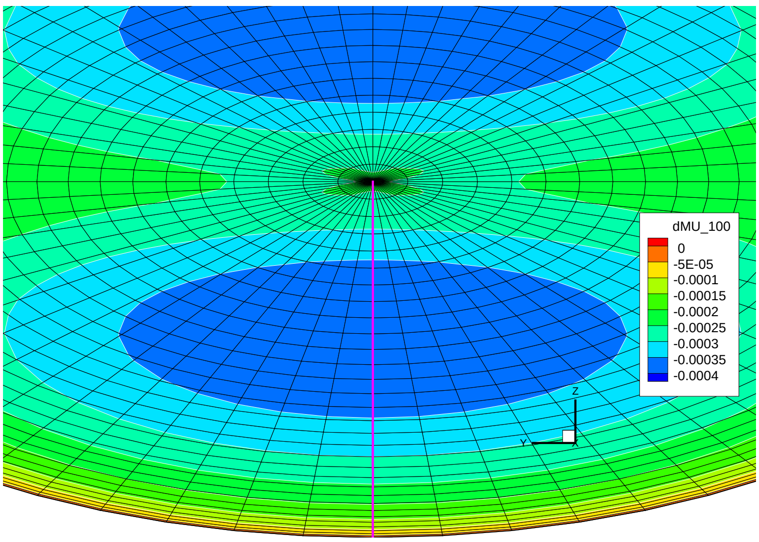

Figure 4.6: Perturbation potential error distribution for a single patch 64×64 panel ellipsoid and an onset flow in x-direction. The largest errors occur outside the poles of the grid.

4.3.2. Six Patch Grid

In Figure 4.7, the variation of the error in the velocity potential is shown as function of characteristic panel size h for the six patch grid. As can be seen, the error is of $\mathcal{O}(h^2)$ in the velocity potential for this panelling. The largest errors appear near areas of large surface curvature, as is shown in Figures 4.8a and 4.8b.

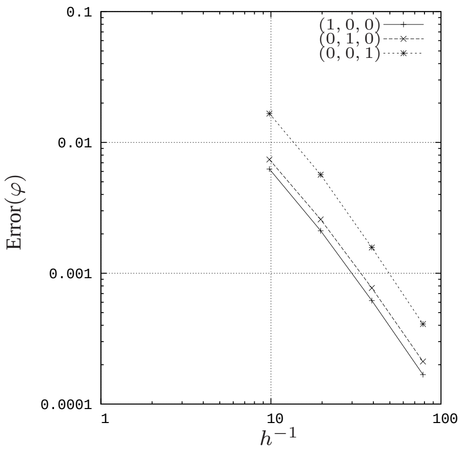

(a) L_1-norms.

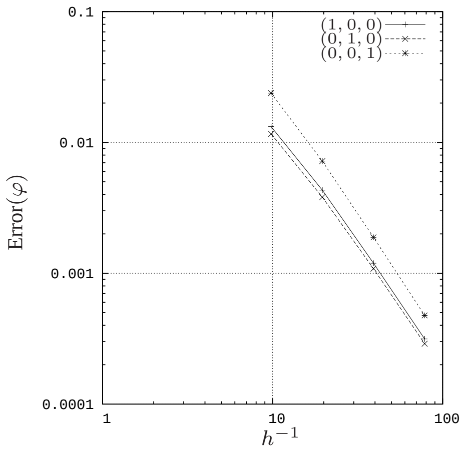

(b) L_2-norms.

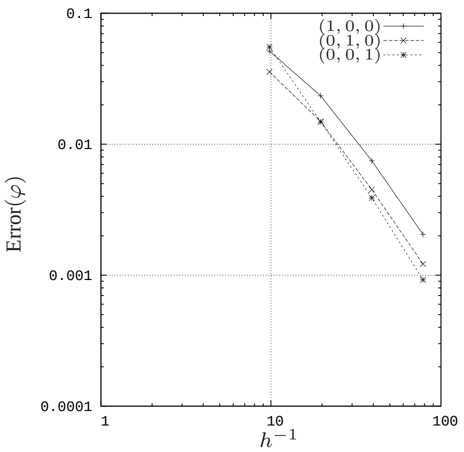

(c) L_∞-norms.

Figure 4.7: Error norms in perturbation potential as a function of h^{-1}, where h is a characteristic panel length, for onset flows along the three coordinate axes of a six patch grid.

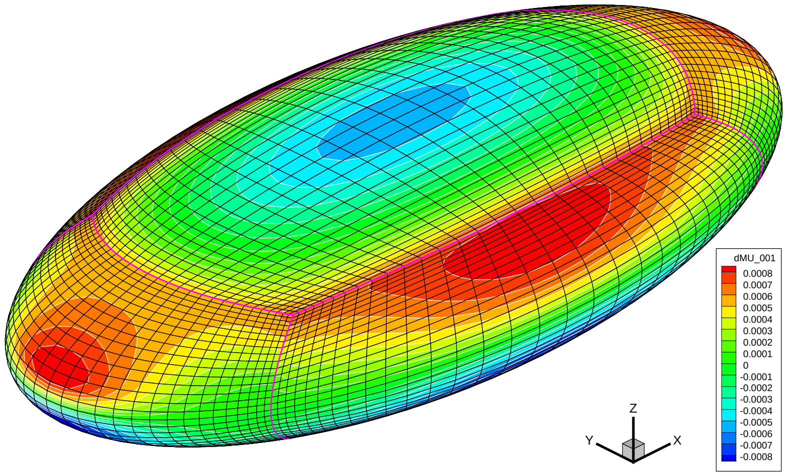

(a) Perturbation potential error.

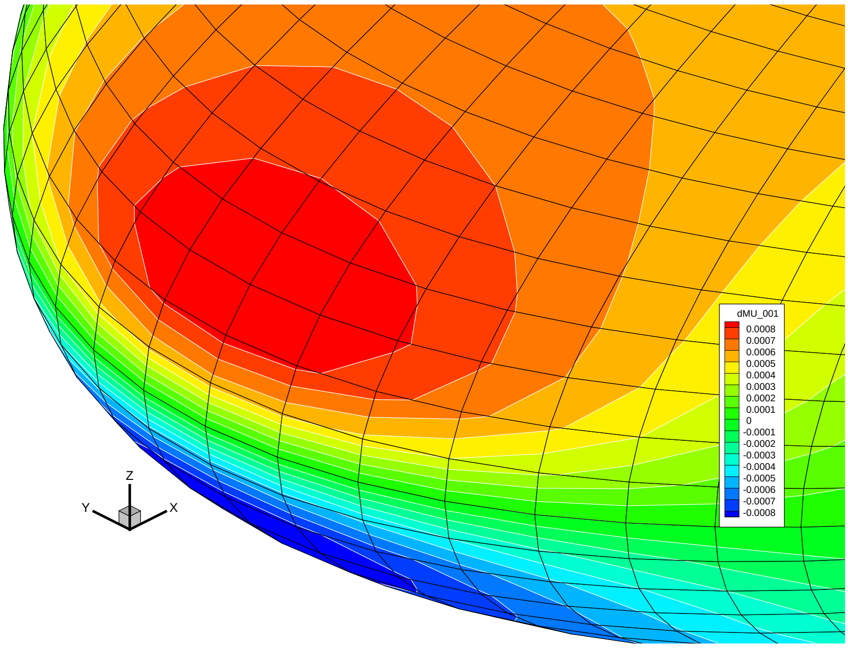

(b) Closeup of a region of large curvature.

Figure 4.8: Perturbation potential error distribution for a six patch $32 \times 32 \times 32$ panel ellipsoid and an onset flow in z-direction.

4.4. Presssure Coefficient Convergence

The pressure coefficients are obtained, via the Bernoulli equation (2.8), from the velocities at the surface. In turn, these velocities are determined in the grid vertices involving a line integral of the perturbation potential through the surrounding collocation points as expressed in equation (3.2.3). At the edges of the grid the velocities are obtained using the potential information of the abutting patch. Two types of panellings are used, one in which the geometry is described by a single patch and one in which six patches are used (see Figure 4.2).

4.4.1. Single Patch Grid

As can be seen in Figure 4.9 the L_1-, L_2- and L_∞ error norms in the pressure coefficient for onset flows along all three coordinate axes show a rate of error reduction of order $\mathcal{O}(h^2)$. It also shows that the largest errors appear for an onset flow in z-direction.

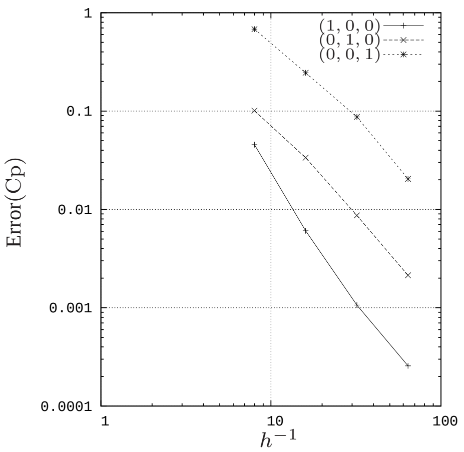

(a) L_1-norm.

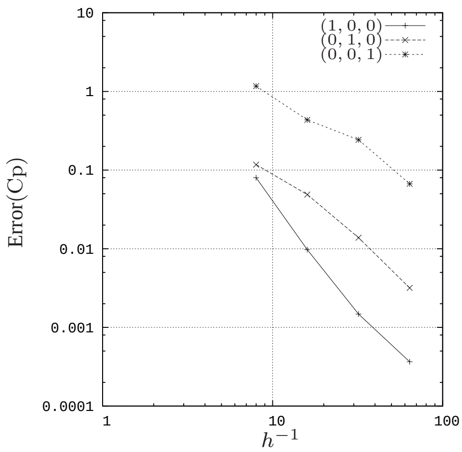

(b) L_2-norm.

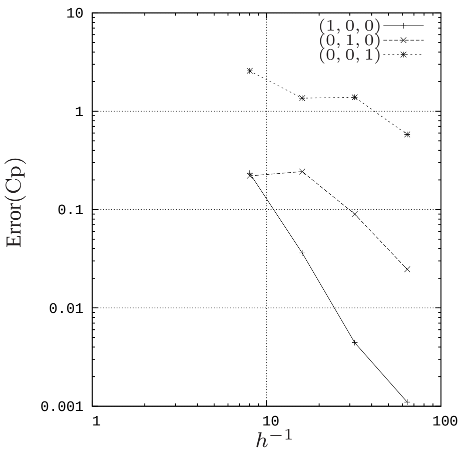

(c) L_∞-norm.

Figure 4.9: Error norms in pressure coefficient as a function of h^{-1}, where h is a characteristic panel length, for onset flows along the three coordinate axes of a single patch grid.

In Figure 4.10, the pressure coefficient error distribution is plotted for an onset flow in z-direction. Because the potential already showed the highest error gradient in the poles of the grid (see Figure 4.4), it is of no surprise that the pressure coefficient error is highest in these poles also.

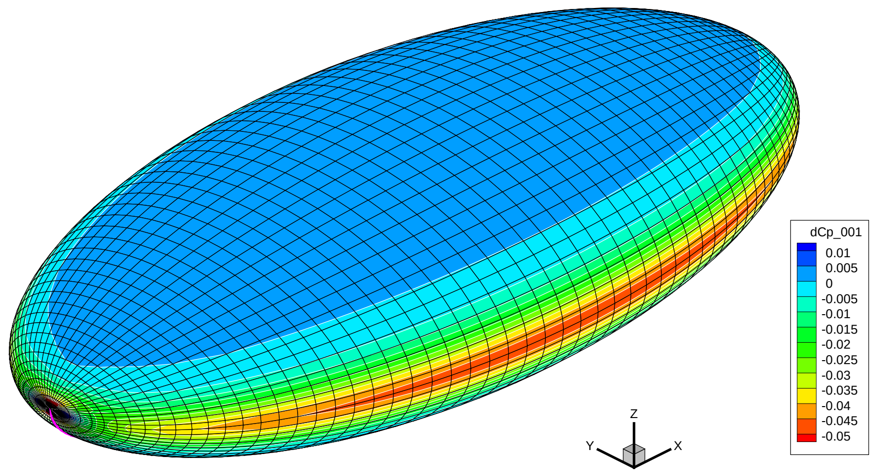

(a) Pressure coefficient error.

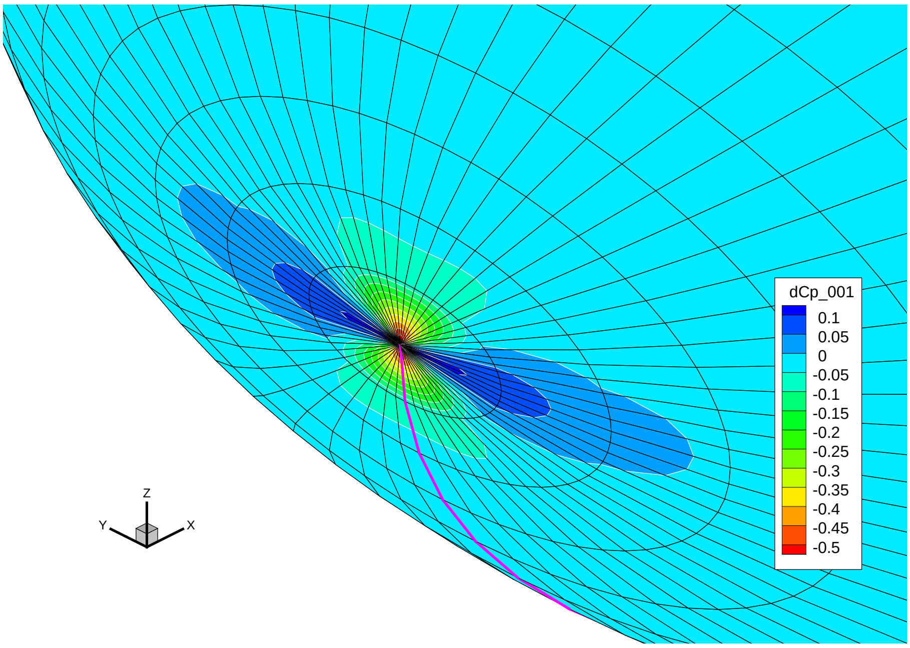

(b) Closeup of the pole region. Note that a different scaling is used.

Figure 4.10: Pressure coefficient error distribution for a 64×64 panel ellipsoid and an onset flow in z-direction. The largest errors appear in the poles of the grid.

4.4.2. Six Patch Grid

In Figure 4.11, the L_1-, L_2- and L_∞ error norms in the pressure coefficient for onset flows along all three coordinate axes are shown for an ellipsoid discretized with a six patch grid. The error is shown to be of order $\mathcal{O}(h^2)$. Notice that the error norms for the six patch grid show a smoother convergence behavior than the single patch in Figure 4.9.

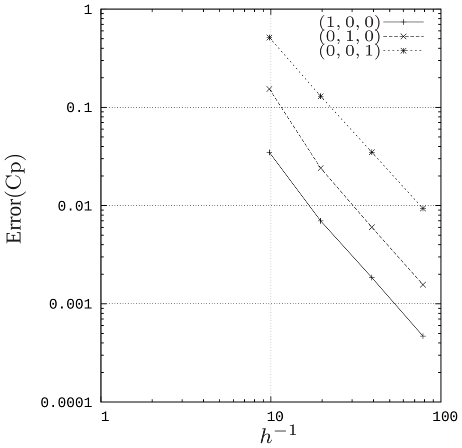

(a) L_1-norm.

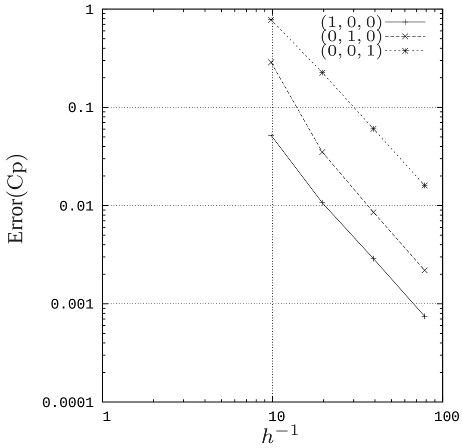

(b) L_2-norm.

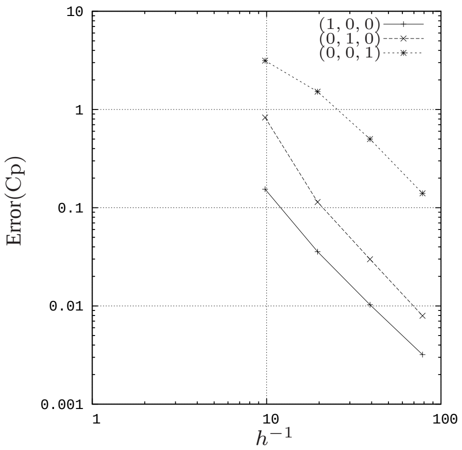

(c) L_∞-norm.

Figure 4.11: Error norms in pressure coefficient as a function of characteristic panel length h, for onset flows along the three coordinate axes of an ellipsoid constructed from six patches.

In Figure 4.12 the pressure coefficient error distribution is plotted for an onset flow in z-direction. The largest errors occur in regions of large curvature where the mesh is relatively coarse. Note that the pressure coefficient distribution itself has highly negative values in the region of highest curvature (see Figure 4.13) at this onset flow condition.

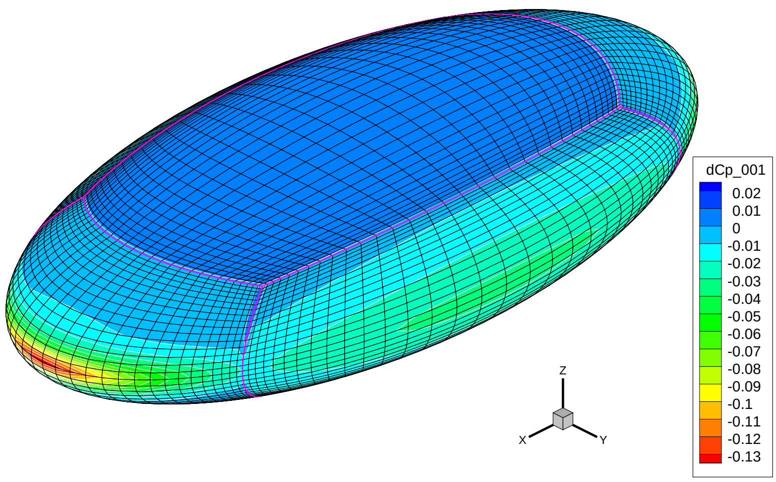

(a) Pressure coefficient error.

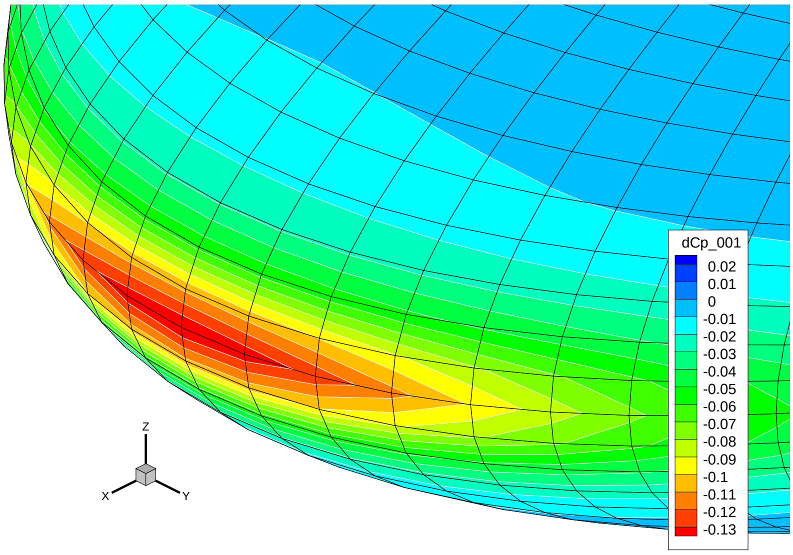

(b) Closeup of a region or large curvature.

Figure 4.12: Pressure coefficient error distribution for a six patch $32 \times 32 \times 32$ panel ellipsoid and an onset flow in z-direction.

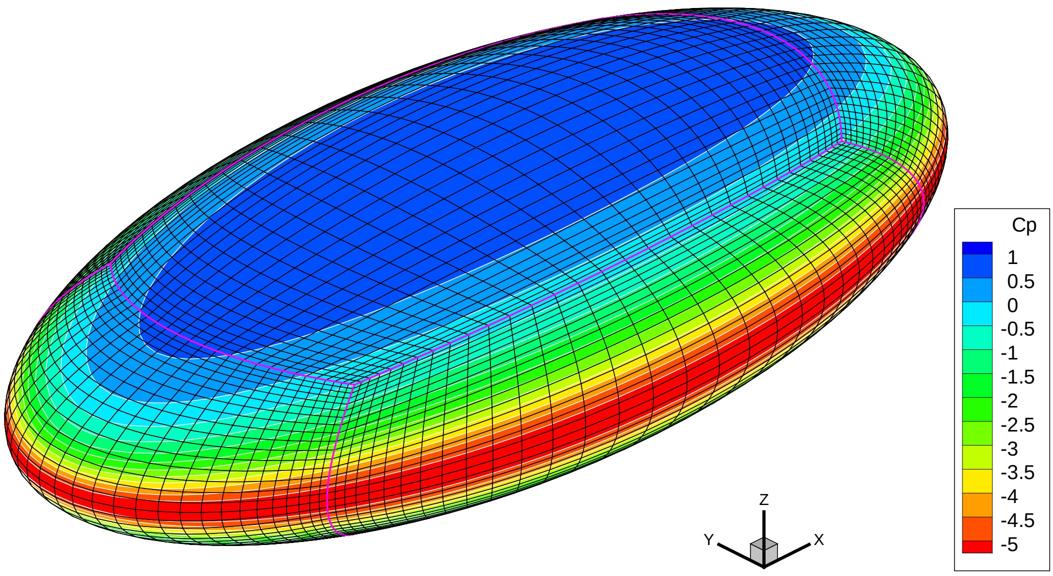

Figure 4.13: Pressure coefficient distribution for a six patch $32 \times 32 \times 32$ panel ellipsoid and an onset flow in z-direction. Note that the minimum values are reached in the region of highest curvature.

5. Application

The current code, designated RotorFlow, can be applied to compute inviscid, incompressible flows around arbitrary 3D lifting and non-lifting bodies in rotating and translating motion. It is unfortunate that for lifting wings in 3D flow no exact analytical testcases exist like those reported in Chapter 4 for the non-lifting tri-axial ellipsoid. The flow solution for a wing of large aspect ratio with an elliptic planform however can be regarded quasi two-dimensional in its center section. This enables us to compare the pressure distribution at that position with a well established 2D airfoil analysis code for steady flow.

5.1. Lifting wing in steady flow

From a modified NACA 0018 airfoil a wing with an elliptic planform was constructed. The span of the elliptic wing was 200 and the root chord was set to 1, giving an aspect ratio of over 254. For this wing the flow at 5 degrees angle-of-attack was simulated and the sectional pressure distribution at half span position was extracted. For the same airfoil section the inviscid pressure distribution at the wing's effective angle-of-attack of 4.961 degrees was computed with the 2D higher order panel code XFOIL from Drela [6]. As shown in Figure 5.1 the XFOIL and the RotorFlow pressure distributions are comparable.

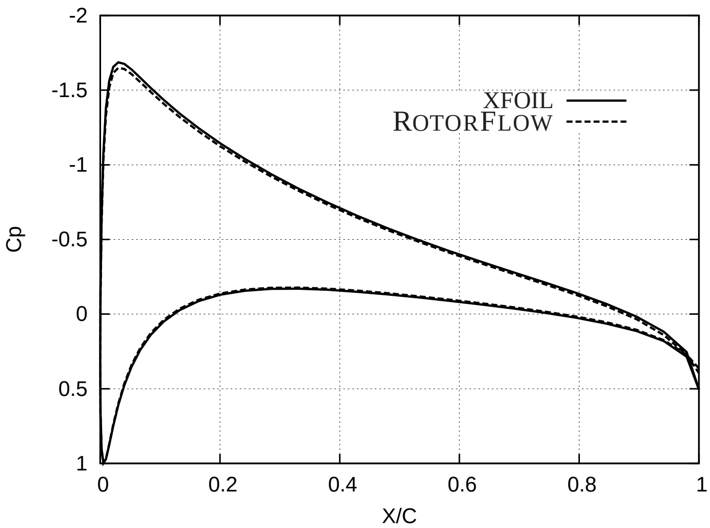

Figure 5.1: Inviscid flow pressure distributions for an airfoil at 5 degrees angle-of-attack.

5.2. Rotating wing in unsteady flow

As a demonstration of the capabilities of the current code the flow solution for a single blade rotor configuration under 30 degrees of yaw was computed where an untwisted elliptic wing was used as blade. For the prescription of the motion of the blade a geometry manipulation approach like the one in the AWSM code [7] was used.

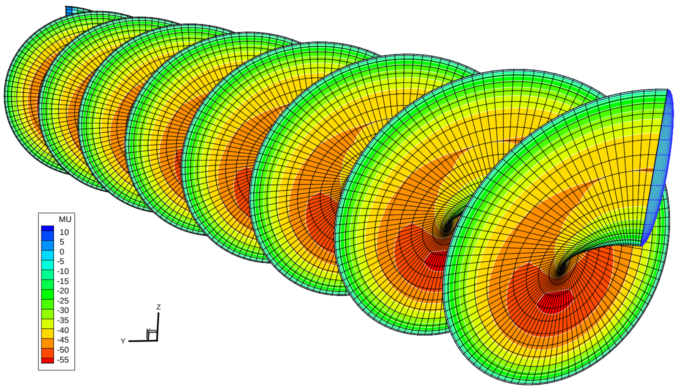

(a) Wake dipole strength development.

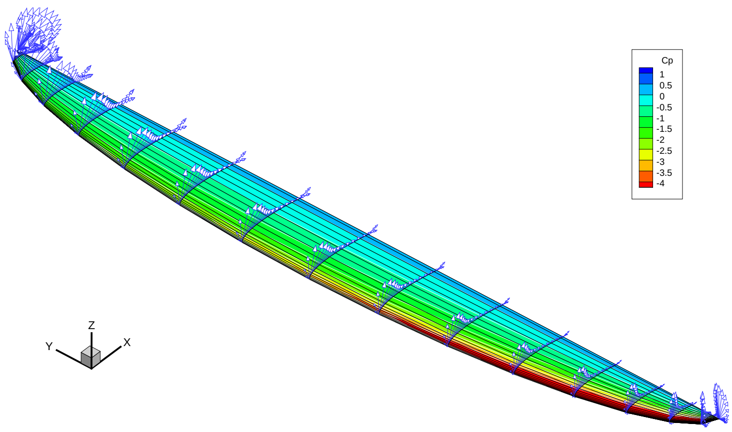

(b) Surface pressure coefficient and velocity vector distibution.

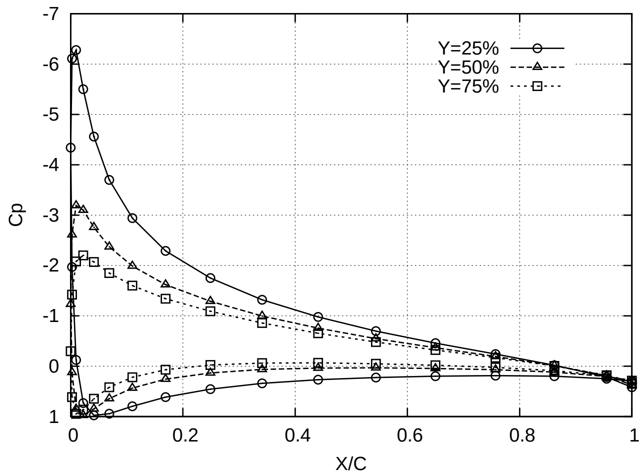

(c) Pressure distribution of sections at 25%, 50%, and 75% blade length.

Figure 5.2: Unsteady flow for a single blade rotor at 30 degrees yaw.

Notice that, due to the lack of blade twist in this blade, the inner airfoil sections experience a higher local angle-of-attack and consequently have a higher suction peak near the nose of the airfoil.

References

[1] W.F. Durand, editor, *Aerodynamic Theory*, Vol. 1, Dover Publications, 1934.

[2] J.D. Anderson, *Fundamentals of Aerodynamics*, McGraw-Hill, fourth ed., 2006.

[3] G.K. Batchelor, *An Introduction to Fluid Dynamics*, Cambridge University Press, 1967.

[4] H.A. Bijleveld, A.E.P. Veldman, *RotorFlow: A quasi-simultaneous interaction for the prediction of aerodynamic flow over wind turbine blades*, In "The Science of Making Torque from Wind", 2010.

[5] G.H. Cottet, P.D. Koumoutsakos, *Vortex Methods: Theory and Practice*, Cambridge University Press, 2000.

[6] M. Drela, *XFOIL: An Analysis and Design System for Low Reynolds Number Airfoils*, In T.J. Mueller, editor, Low Reynolds Number Aerodynamics, Vol. 54 of *Lecture Notes in Engineering*, pages 1–12. Springer-Verlag, New York, 1989.

[7] A. van Garrel, *Development of a Wind Turbine Aerodynamics Simulation Module*, ECN-C--03-079, Energy research Centre of the Netherlands, 2003.

[8] A. van Garrel, *Integral Boundary Layer Methods for Wind Turbine Aerodynamics*, ECN-C--04-004, Energy research Centre of the Netherlands, 2004.

[9] H.W.M. Hoeijmakers, *Panel Methods for Aerodynamic Analysis and Design*, In "Special Course on Engineering Methods in Aerodynamic Analysis and Design of Aircraft", AGARD Report R-783, 1991.

[10] J. Katz, A. Plotkin, *Low-Speed Aerodynamics: From Wing Theory to Panel Methods*, Cambridge University Press, second ed., 2001.

[11] H. Lamb, *Hydrodynamics*, Cambridge University Press, sixth ed., 1932.

[12] L. Morino, C.-C. Kuo, *Subsonic Potential Aerodynamics for Complex Configurations: A General Theory*, AIAA J., 12(2):191–197, 1974.

[13] H. Özdemir, E.F. van den Boogaard, *Solving the integral boundary layer equations with a discontinuous Galerkin method*, EWEA 2011, 2011.

[14] P.G. Saffman, *Vortex Dynamics*, Cambridge Monographs on Mechanics and Applied Mathematics, Cambridge University Press, 1992.

A. Mathematical Compendium

This chapter contains a collection of some useful mathematical formulas. In index notation formulas summation over repeated indices is assumed.

Divergence Theorem: The Divergence Theorem is Gauß' theorem for a vector function $\vec{b}$ and relates the volume and surface integrals of the vector field in a volume V enclosed by the surface ∂V by:

$$\iiint\limits_V (\nabla \cdot \vec{b}) \, dV = \iint\limits_{\partial V} \vec{b} \cdot \bar{n} \, dS.$$

Gauß' Theorem: Gauß' theorem gives a relation between the volume and surface integrals of a continuously differentiable (i.e. C^1 functions with continuous derivative) arbitrary tensor function T_{ij} over a volume V enclosed by piecewise smooth boundary ∂V with outward unit normal vector $\bar{n}$. The tensor T_{jk} may be a scalar, vector or tensor function of any rank. In index notation Gauß' theorem reads:

$$\iiint\limits_V \partial_i (T_{jk}) \, dV = \iint\limits_{\partial V} n_i \, T_{jk} \, dS.$$

Some special forms of Gauß' theorem are obtained when specific choices are substituted for tensor T_{jk}. Substituting vector field b_i for T_{jk} for example gives the Divergence Theorem and when scalar field ϕ is substituted for T_{jk} we arrive at the Gradient Theorem.

Substitution of $\epsilon_{kij} b_j$ for tensor T_{jk} gives

$$\iiint\limits_V (\nabla \times \vec{b}) \, dV = \iint\limits_{\partial V} (\bar{n} \times \vec{b}) \, dS.$$

Gradient Theorem: The Gradient Theorem is Gauß' theorem for a scalar function ϕ and relates the volume and surface integrals of the scalar field over a volume V enclosed by the surface ∂V by:

$$\iiint\limits_V (\nabla \phi) \, dV = \iint\limits_{\partial V} \phi \bar{n} \, dS$$

Green's identities: One of Green's identities is obtained when $\epsilon_{kij} b_j$ is substituted for T_{jk} in Gauß' theorem. Combined over all components k this leads to:

$$\iiint\limits_V (\nabla \times \vec{b}) \, dV = \iint\limits_{\partial V} (\bar{n} \times \vec{b}) \, dS.$$

Green's first identity is obtained when $(\psi \, \partial_i \phi)$ is substituted into Gauß' theorem for T_{jk}, where ψ and ϕ are once and twice continuously differentiable scalar functions respectively:

$$\iiint\limits_V \psi \nabla^2 \phi \, dV = \iint\limits_{\partial V} \psi \frac{\partial \phi}{\partial n} \, dS - \iiint\limits_V \nabla \phi \cdot \nabla \psi \, dV,$$

where $\partial\phi/\partial n = \nabla\phi \cdot \bar{n}$ denotes the derivative in the direction of the outward normal and $\nabla^2{=}\nabla{\cdot}\nabla$ is the Laplacian operator.

Green's second identity is obtained from the first identity by interchanging the role of ψ and ϕ and subtract the resulting equations. Now both ψ and ϕ are assumed twice continuously differentiable scalar functions. Green's second identity reads:

$$\iiint\limits_V \left(\psi\nabla^2\phi - \phi\nabla^2\psi\right)\, dV = \iint\limits_{\partial V} \left(\psi\frac{\partial\phi}{\partial n} - \phi\frac{\partial\psi}{\partial n}\right)\, dS.$$

Stokes' Theorem: Stokes' theorem relates the line integral of a smooth vector field $\vec{b}$ over a closed curve ∂S to the surface integral of $\vec{b}$ over an open surface S bounded by curve ∂S. The orientations of unit tangent vector $\bar{\tau}$ to curve ∂S and the unit normal vector $\bar{n}$ to surface S are related through the right hand rule.

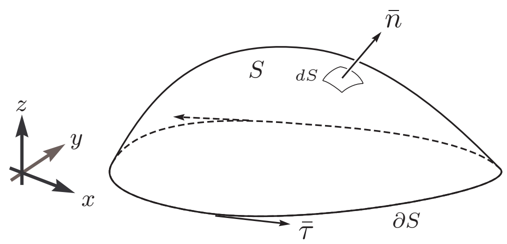

Stokes' theorem reads:

$$\iint\limits_S (\nabla{\times}\vec{b}) \cdot \bar{n}\; dS = \int\limits_{\partial S} \vec{b} \cdot \bar{\tau}\; ds.$$

Substantial derivative: The substantial derivative, also know as material derivative, is the time rate of change following a fluid element moving with velocity $\vec{u}$, and can be split into the local and the convective derivative:

$$\frac{\mathrm{D}}{\mathrm{D}t} = \frac{\partial}{\partial t} + \vec{u} \cdot \nabla.$$

Vector identities:

$$
\begin{aligned}
\vec{a}\cdot(\vec{b}\times\vec{c}) &= \vec{b}\cdot(\vec{c}\times\vec{a}) \;=\; \vec{c}\cdot(\vec{a}\times\vec{b}) \\
\vec{a}\times(\vec{b}\times\vec{c}) &= \vec{b}\,(\vec{a}\cdot\vec{c}) - \vec{c}\,(\vec{a}\cdot\vec{b}) \\
(\vec{a}\times\vec{b})\times\vec{c} &= \vec{b}\,(\vec{a}\cdot\vec{c}) - \vec{a}\,(\vec{b}\cdot\vec{c}) \\
(\vec{a}\times\vec{b})\cdot(\vec{c}\times\vec{d}) &= (\vec{a}\cdot\vec{c})(\vec{b}\cdot\vec{d}) - (\vec{a}\cdot\vec{d})(\vec{b}\cdot\vec{c}) \\
(\vec{a}\times\vec{b})\times(\vec{c}\times\vec{d}) &= \vec{c}\,(\vec{a}\cdot(\vec{b}\times\vec{d})) - \vec{d}\,(\vec{a}\cdot(\vec{b}\times\vec{c})) \\
&= \vec{b}\,(\vec{a}\cdot(\vec{c}\times\vec{d})) - \vec{a}\,(\vec{b}\cdot(\vec{c}\times\vec{d})) \\
\vec{x} &= \tfrac{\vec{x}\cdot(\vec{b}\times\vec{c})}{\vec{a}\cdot(\vec{b}\times\vec{c})}\vec{a} + \tfrac{\vec{x}\cdot(\vec{c}\times\vec{a})}{\vec{a}\cdot(\vec{b}\times\vec{c})}\vec{b} + \tfrac{\vec{x}\cdot(\vec{a}\times\vec{b})}{\vec{a}\cdot(\vec{b}\times\vec{c})}\vec{c} \\
\nabla(fg) &= f(\nabla g) + g(\nabla f) \\
\nabla(\vec{a}\cdot\vec{b}) &= \vec{a}\times(\nabla\times\vec{b}) + \vec{b}\times(\nabla\times\vec{a}) + (\vec{a}\cdot\nabla)\vec{b} + (\vec{b}\cdot\nabla)\vec{a} \\
\nabla\cdot(f\vec{a}) &= f(\nabla\cdot\vec{a}) + \vec{a}\cdot(\nabla f) \\
\nabla\cdot(\vec{a}\times\vec{b}) &= \vec{b}\cdot(\nabla\times\vec{a}) - \vec{a}\cdot(\nabla\times\vec{b}) \\
\nabla\times(\vec{a}\times\vec{b}) &= (\vec{b}\cdot\nabla)\,\vec{a} - (\vec{a}\cdot\nabla)\,\vec{b} + \vec{a}\,(\nabla\cdot\vec{b}) - \vec{b}\,(\nabla\cdot\vec{a}) \\
\nabla\times(f\vec{a}) &= f\,(\nabla\times\vec{a}) + \nabla f\times\vec{a} \\
\nabla\times(\nabla\times\vec{a}) &= \nabla(\nabla\cdot\vec{a}) - (\nabla\cdot\nabla)\,\vec{a} \\
\vec{a}\cdot((\vec{b}\times\nabla)\times\vec{c}) &= ((\vec{a}\cdot\nabla)\,\vec{c})\cdot\vec{b} - (\vec{a}\cdot\vec{b})(\nabla\cdot\vec{c}) \\
\nabla\cdot(\nabla\times\vec{a}) &= 0 \\
\nabla\cdot(\nabla f\times\nabla g) &= 0 \\
\nabla\times\nabla f &= \vec{0}
\end{aligned}
$$

B. Conservation Laws

In this chapter the derivation of the conservation laws for mass and momentum is given for reasons of completeness. It can be found in textbooks on fluid mechanics. A clear explanation is for example given in reference [2].

B.1. Mass Conservation

Let us consider an arbitrary control volume V fixed in space where fluid is freely flowing with velocity $\vec{u}(\vec{x},t)$ through its bounding surface ∂V with unit normal vector $\bar{n}(\vec{x})$ pointing outward as shown in Figure B.1. The equation for mass conservation, also known as the continuity equation, expresses that an increase in mass in volume V can only come from a net mass flow through its bounding surface ∂V

$$\frac{\mathrm{d}}{\mathrm{d}t}(\text{Mass in } V) = \text{Net mass inflow per unit time.}$$

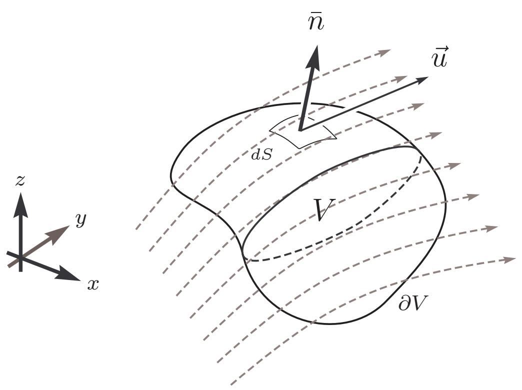

Figure B.1: A control volume V fixed in space with fluid freely flowing through its bounding surface ∂V.

Considering that $\vec{u} \cdot \bar{n}\, dS$ is the volume that flows out of area dS per unit time, we can write for the net mass flowing through the surface into control volume V per unit time:

$$\text{Mass inflow} = -\iint\limits_{\partial V} \rho \vec{u} \cdot \bar{n}\, dS,$$

where $\rho(\vec{x},t)$ is the mass density of the fluid and the minus sign comes from the fact that we defined the normal as positive when pointing outward. The integral form of the equation for mass conservation can now be written as

$$\frac{\mathrm{d}}{\mathrm{d}t}\iiint\limits_{V} \rho\, dV + \iint\limits_{\partial V} \rho \vec{u} \cdot \bar{n}\, dS = 0. \tag{B.1}$$

We can use the Divergence Theorem to transform the surface integral into a volume integral, provided we have a continuously differentiable vector field $\rho\vec{u}$:

$$\frac{\mathrm{d}}{\mathrm{d}t}\iiint\limits_V \rho\, dV + \iiint\limits_V \nabla\cdot(\rho\vec{u})\, dV = 0,$$

which can be written as

$$\iiint\limits_V \left(\frac{\partial\rho}{\partial t} + \nabla\cdot(\rho\vec{u})\right) dV = 0,$$

where we used the fact that our control volume was fixed in space to shift the time derivative to the integrand. Because this equation is valid for arbitrary control volumes, the integrand has to be zero for any point within V, and we arrive at the differential form of the continuity equation

$$\frac{\partial\rho}{\partial t} + \nabla\cdot(\rho\vec{u}) = 0, \tag{B.2}$$

which can also be written as

$$\nabla\cdot\vec{u} = -\frac{1}{\rho}\frac{\mathrm{D}\rho}{\mathrm{D}t}. \tag{B.3}$$

For incompressible flow the mass density ρ of fluid particles is constant and equation (B.2) reduces to a form without time derivative term

$$\nabla\cdot\vec{u} = 0. \tag{B.4}$$

If we now additionally assume irrotational flow $\nabla\times\vec{u} = \vec{0}$, we can write the velocity vector as the gradient of a scalar function $\Phi(\vec{x}, t)$, that is

$$\vec{u} = \nabla\Phi. \tag{B.5}$$

Substitution of this expression for the velocity vector into the continuity equation (B.4) results in the Laplace equation for the unknown velocity potential Φ:

$$\nabla\cdot\nabla\Phi \;=\; \frac{\partial^2\Phi}{\partial x^2} + \frac{\partial^2\Phi}{\partial y^2} + \frac{\partial^2\Phi}{\partial z^2} \;=\; 0. \tag{B.6}$$

B.2. Momentum Conservation

Momentum conservation is expressed by Newton's second law of motion that states that, viewed from an inertial frame of reference, the time rate of change of the linear momentum of a particle is proportional to the net force excerted on it:

$$\frac{\mathrm{d}}{\mathrm{d}t}(m\vec{u}) = \vec{F},$$

where m is the mass of the particle and $\vec{u}$ its velocity.

Using our fixed control volume from Figure B.1, the equation for momentum conservation expresses that an increase in momentum in volume V can only come from a net momentum flow through its surface or from a force excerted on the fluid. The equation for conservation of linear momentum can be written symbolically as

$$\frac{\mathrm{d}}{\mathrm{d}t}(\text{Momentum in } V) = \text{Net momentum inflow per unit time } + \vec{F}$$

For the net momentum flowing through the surface into the control volume per unit time we can write

$$\text{Momentum inflow} = -\iint\limits_{\partial V} \rho\vec{u}(\vec{u}\cdot\bar{n})\, dS,$$

where the minus sign comes from the definition of the unit surface normal as positive when pointing outward. The momentum equation can now be written in integral form as

$$\frac{\mathrm{d}}{\mathrm{d}t}\iiint\limits_{V} \rho\vec{u}\, dV + \iint\limits_{\partial V} \rho\vec{u}(\vec{u}\cdot\bar{n})\, dS = \vec{F}, \tag{B.7}$$

The force $\vec{F}$ acting on the fluid can be split into body forces that act upon the mass inside the control volume, and forces that act on the surface of the volume. Body forces are of the form

$$\vec{F}_{body} = \iiint\limits_{V} \rho\vec{f}dV, \tag{B.8}$$

where $\vec{f}$ is defined as the force per unit mass. An example of such a body force is the force caused by gravity. With the gravitational accelleration vector denoted by $\vec{g}$ we can write this body force as

$$\vec{F}_{gravity} = \iiint\limits_{V} \rho\vec{g}\, dV. \tag{B.9}$$

The forces that act on the surface of the control volume can be decomposed into a force due to the static pressure p acting on surface ∂V in normal direction

$$\vec{F}_{pressure} = -\iint\limits_{\partial V} p\bar{n}\, dS, \tag{B.10}$$

and a force due to the viscosity of the fluid

$$\vec{F}_{viscous} = \iint\limits_{\partial V} \vec{\tau}\, dS = \iint\limits_{\partial V} \bar{\bar{\tau}}\cdot\bar{n}\, dS. \tag{B.11}$$

Including the forces due to gravity (B.9), pressure (B.10) and viscosity (B.11) in the momentum conservation equations (B.7) results in

$$\frac{\mathrm{d}}{\mathrm{d}t}\iiint\limits_{V} \rho\vec{u}\, dV + \iint\limits_{\partial V} \rho\vec{u}(\vec{u}\cdot\bar{n})\, dS = \iiint\limits_{V} \rho\vec{g}\, dV - \iint\limits_{\partial V} p\bar{n}\, dS + \iint\limits_{\partial V} \bar{\bar{\tau}}\cdot\bar{n}\, dS. \tag{B.12}$$

We can use the Divergence Theorem and Gradient Theorem to transform the surface integrals in equation (B.12) into volume integrals, provided we have a continuously differentiable tensor field $\rho\vec{u}\vec{u}$, pressure field p, and stress tensor field $\bar{\bar{\tau}}$, giving

$$\iiint\limits_{V} \left(\frac{\partial(\rho\vec{u})}{\partial t} + \nabla\cdot(\rho\vec{u}\vec{u}) + \nabla p - \rho\vec{g} - \nabla\cdot\bar{\bar{\tau}}\right) dV = \vec{0},$$

where we used the fact that the control volume is fixed and we are allowed to shift the time derivative to the integrand. Because this equation is valid for arbitrary control volumes, the integrand on the left hand side has to balance the right hand side everywhere within V, and we arrive at the differential form of the momentum equations:

$$\frac{\partial(\rho\vec{u})}{\partial t} + \nabla\cdot(\rho\vec{u}\vec{u}) + \nabla p - \rho\vec{g} - \nabla\cdot\bar{\bar{\tau}} = \vec{0}. \tag{B.13}$$

For Newtonian fluids the viscous stresses are considered to be proportional to velocity gradients through the constitutive relation

$$\bar{\bar{\tau}} = \mu \left[\nabla \vec{u} + (\nabla \vec{u})^{\mathrm{T}} - \frac{2}{3} (\nabla \cdot \vec{u}) \, \bar{\bar{I}} \right], \tag{B.14}$$

where the dynamic viscosity coefficient μ is in general a function of temperature.

This result can be simplified considerably if we assume the flow to be inviscid and incompressible. Additionally, we write the constant gravitational acceleration vector $\vec{g}$ as the gradient of scalar function h, the height above the ground, $\vec{g} = -g \nabla h$, where the minus sign comes from ∇h having the opposite direction of $\vec{g}$. The constant mass density allows us then to combine the pressure and gravitational terms in equation (B.13) and, using the continuity equation (B.4) for incompressible flows, we arrive at the differential form of the momentum equations for inviscid, incompressible flows:

$$\rho \frac{\partial \vec{u}}{\partial t} + \rho (\vec{u} \cdot \nabla) \vec{u} + \nabla (p + \rho g h) = \vec{0}. \tag{B.15}$$

Using one of the vector identities from appendix A, the second term in above equation can be witten as

$$(\vec{u} \cdot \nabla) \vec{u} = \nabla (\frac{1}{2} \vec{u} \cdot \vec{u}) - \vec{u} \times (\nabla \times \vec{u}). \tag{B.16}$$

Assuming steady flow, the substitution of the vector identity B.16 in the momentum equations B.15 for inviscid, incompressible flow gives

$$\nabla \left(\frac{1}{2} \vec{u} \cdot \vec{u} + \frac{p}{\rho} + g h \right) = \vec{u} \times (\nabla \times \vec{u}),$$

and taking the inner product with velocity vector $\vec{u}$ results in

$$\vec{u} \cdot \nabla \left(\frac{1}{2} \vec{u} \cdot \vec{u} + \frac{p}{\rho} + g h \right) = 0,$$

which gives us the Bernoulli equation for steady, incompressible, inviscid, and rotational flow that is valid in every point on a streamline through $\vec{x}_0$:

$$\frac{1}{2} \vec{u} \cdot \vec{u} + \frac{p}{\rho} + g h = C(\vec{x}_0). \tag{B.17}$$

Let us start again with the momentum equations for unsteady, inviscid, incompressible flow B.15, and assume an irrotational velocity field $\nabla \times \vec{u} = \vec{0}$. We can now introduce $\vec{u} = \nabla \Phi$, and with the use of vector identity B.16 arrive at

$$\nabla \left(\rho \frac{\partial \Phi}{\partial t} + \frac{1}{2} \rho \nabla \Phi \cdot \nabla \Phi + p + \rho g h \right) = \vec{0},$$

which gives the Bernoulli equation for unsteady, incompressible, potential flow:

$$\frac{\partial \Phi}{\partial t} + \frac{1}{2} \nabla \Phi \cdot \nabla \Phi + \frac{p}{\rho} + g h = C(t). \tag{B.18}$$

B.3. Energy Conservation

The equation for energy conservation is based on the first law of thermodynamics that states that an increase in total energy in a volume V per unit time can only come from the energy added by heat per unit time or from the work per unit time done by forces. Using the fixed control volume from Figure B.1, the equation for energy conservation for fluid flows can be expressed symbolically by

$$\frac{\mathrm{d}}{\mathrm{d}t}(\text{Energy in } V) = \text{Net energy inflow per unit time} \ + \ \dot{\text{Heat}} \ + \ \dot{\text{Work}}.$$

Let $E(\vec{x}, t)$ be the total specific energy, that is the total energy per unit mass, and let $e(\vec{x}, t)$ be the internal specific energy that comes from molecular motion. The total specific energy is the sum of the internal specific energy and the kinetic specific energy that is associated with the bulk velocity $\vec{u}(\vec{x}, t)$, that is

$$E = e + \frac{1}{2}\vec{u} \cdot \vec{u}. \tag{B.19}$$

The total energy in volume V is

$$\text{Energy in } V = \iiint_V \rho E \, dV.$$

For the net energy flowing through the surface ∂V into the control volume per unit time we can write

$$\text{Energy inflow} = -\iint_{\partial V} \rho E(\vec{u} \cdot \bar{n}) \, dS,$$

where the minus sign comes from the definition of the unit surface normal as positive when pointing outward. The expression for energy conservation can now be written as

$$\frac{\mathrm{d}}{\mathrm{d}t} \iiint_V \rho E \, dV + \iint_{\partial V} \rho E(\vec{u} \cdot \bar{n}) \, dS = \ \dot{\text{Heat}} \ + \ \dot{\text{Work}}. \tag{B.20}$$

The heat that is added to the volume can be split into body heating that acts on the fluid inside the volume, and surface heating that acts through thermal conduction and is caused by gradients in the heat distribution. Let $\dot{Q}(\vec{x}, t)$ denote the body heat in Joule per unit volume per unit time, and let $\vec{q}$ be the heat flux vector in Joule per unit area per unit time, then

$$\text{Body heating} \quad = \quad \iiint_V \dot{Q} \, dV, \tag{B.21}$$

$$\text{Surface heating} \quad = \quad -\iint_{\partial V} \vec{q} \cdot \bar{n} \, dS. \tag{B.22}$$

In general, for the work done per unit time by applying a force $\vec{f}(\vec{x}, t)$ to the fluid moving with velocity $\vec{u}(\vec{x}, t)$ we can write

$$\dot{\mathrm{W}}_{force} = \vec{f} \cdot \vec{u}$$

The forces can be split into body forces that act upon the mass inside the volume, and forces that act on the surface of the volume, see Appendix B.2.

An example of a body force is the gravitational force. With the gravitational accelleration vector denoted by $\vec{g}$ we can write the work done per unit time by this body force as

$$\dot{\mathrm{W}}_{gravity} = \iiint_V \rho \vec{g} \cdot \vec{u} \, dV. \tag{B.23}$$

The forces that act on the surface of the control volume can be decomposed into a force in normal direction due to the static pressure $p(\vec{x},t)$ acting on surface ∂V and a force due to the viscosity of the fluid. The work done by the static pressure per unit time is

$$\dot{\mathrm{W}}_{pressure} = -\iint\limits_{\partial V} p\vec{u}\cdot\bar{n}\,dS, \tag{B.24}$$

and for the work done by viscous forces per unit time we have

$$\dot{\mathrm{W}}_{viscous} = \iint\limits_{\partial V} \vec{\tau}\cdot\vec{u}\,dS = \iint\limits_{\partial V} (\bar{\bar{\tau}}\cdot\vec{u})\cdot\bar{n}\,dS. \tag{B.25}$$

Combining all heat and work contributions in the expression for energy conservation B.20 results in the energy equation in integral form:

$$\begin{aligned}\frac{\mathrm{d}}{\mathrm{d}t}\iiint\limits_{V}\rho E\,dV + \iint\limits_{\partial V}\rho E(\vec{u}\cdot\bar{n})\,dS \quad &= \quad -\iint\limits_{\partial V} p\vec{u}\cdot\bar{n}\,dS + \iiint\limits_{V}\rho\vec{g}\cdot\vec{u}\,dV \\ &+ \quad \iiint\limits_{V} Q\,dV - \iint\limits_{\partial V}\vec{q}\cdot\bar{n}\,dS \\ &+ \quad \iint\limits_{\partial V}(\bar{\bar{\tau}}\cdot\vec{u})\cdot\bar{n}\,dS. \end{aligned} \tag{B.26}$$

We can use the Divergence Theorem to convert the surface integrals to volume integrals, provided we have continuously differentiable vector fields $\rho E\vec{u}$, $p\vec{u}$, $\vec{q}$, and $\bar{\bar{\tau}}\cdot\vec{u}$, and arrive at

$$\begin{aligned}\iiint\limits_{V}\frac{\partial(\rho E)}{\partial t}\,dV + \iiint\limits_{V}\nabla\cdot(\rho E\vec{u})\,dV \quad &= \quad \iiint\limits_{V}\nabla\cdot(p\vec{u})\,dV + \iiint\limits_{V}\rho\vec{g}\cdot\vec{u}\,dV \\ &+ \quad \iiint\limits_{V} Q\,dV - \iiint\limits_{V}\nabla\cdot\vec{q}\,dV \\ &+ \quad \iiint\limits_{V}\nabla\cdot(\bar{\bar{\tau}}\cdot\vec{u})\,dV, \end{aligned} \tag{B.27}$$

where we used the fact that the control volume is fixed and we are allowed to shift the time derivative to the integrand. Because this equation is valid for arbitrary control volumes, the integrals have to balance each other everywhere in volume V and consequently the equation can be written in differential form:

$$\frac{\partial(\rho E)}{\partial t} + \nabla\cdot(\rho E\vec{u}) + \nabla\cdot(p\vec{u}) - \rho\vec{g}\cdot\vec{u} - Q + \nabla\cdot\vec{q} - \nabla\cdot(\bar{\bar{\tau}}\cdot\vec{u}) = 0. \tag{B.28}$$

We can rewrite above energy equation in terms of total specific enthalphy $H(\vec{x},t)$ which is defined as

$$H = E + \frac{p}{\rho}. \tag{B.29}$$

The substitution of the definition for total specific enthalphy in energy equation B.28 gives a simpler enthalphy equation that does not explicitly contain the pressure work term:

$$\frac{\partial(\rho H)}{\partial t} + \nabla\cdot(\rho H\vec{u}) = \frac{\partial p}{\partial t} + \rho\vec{g}\cdot\vec{u} + Q - \nabla\cdot\vec{q} + \nabla\cdot(\bar{\bar{\tau}}\cdot\vec{u}). \tag{B.30}$$

Expanding the term on the left hand side of the equation, and making use of the continuity equation B.2, the non-conservative form of the equation for total enthalphy H is obtained

$$\rho \frac{\mathrm{D}H}{\mathrm{D}t} = \frac{\partial p}{\partial t} + \rho \vec{g} \cdot \vec{u} + Q - \nabla\cdot\vec{q} + \nabla\cdot(\bar{\bar{\tau}} \cdot \vec{u}). \tag{B.31}$$

The energy equation is supplemented with two equations of state and two constitutive relations, one for stress tensor $\bar{\bar{\tau}}(\vec{x}, t)$ and one for heat flux vector $\vec{q}(\vec{x}, t)$. A model for the heat flux vector is given by Fourier's law

$$\vec{q} = -\kappa \nabla T,$$

where κ is the heat conduction coefficient, and $T(\vec{x}, t)$ the temperature field.

The constitutive relation for the stress tensor was introduced in the derivation of the momentum equations in Appendix B.2 and is

$$\bar{\bar{\tau}} = \mu \left[\nabla\vec{u} + (\nabla\vec{u})^{\mathrm{T}} - \frac{2}{3}(\nabla\cdot\vec{u})\, \bar{\bar{I}} \right],$$

with μ the dynamic viscosity coefficient that is in general a function of temperature T.

Two equations of state complement the energy equation: one expressing the relation between pressure p, mass density ρ, and temperature T, and one expression for the specific internal energy e. For a calorically perfect gas the two equations of state are

$$p = \rho R T,$$

with R the specific gas constant which for air is approximately $R = 287$ Joule per kilogram per Kelvin, and

$$e = c_v T,$$

with c_v the specific heat at constant volume.

Related to these two expressions and the definition of specific enthalpy $h = e + \frac{p}{\rho}$ is the relation

$$h = c_p T,$$

with c_p the specific heat at constant pressure. The ratio between the two specific heats is denoted by $\gamma = \frac{c_p}{c_v}$ and is for air $\gamma = 1.4$.

C. Boundary Integral Equation

In an inertial Cartesian coordinate system in which coordinates are denoted by $\vec{x} = (x, y, z)^{\mathrm{T}}$, the Laplace equation for the velocity potential in unsteady, incompressible flow, in domain $V \in \mathbb{R}^3$, can be written as

$$\nabla\cdot\nabla\Phi = \frac{\partial^2\Phi}{\partial x^2} + \frac{\partial^2\Phi}{\partial y^2} + \frac{\partial^2\Phi}{\partial z^2} = 0 \tag{C.1}$$

Although the Laplace equation has no time-dependent term, the velocity potential $\Phi(\vec{x}, t)$ is a function of space and time. Unsteady boundary conditions will introduce time-dependency in the solution. In this section, this time-dependency is implicitly assumed. The problem in volume V can be reduced to a problem involving only surface integrals by the introduction of a special form of the Divergence Theorem that relates the volume and surface integrals of an arbitrary tensor function over a volume V enclosed by surface ∂V with unit normal vector $\bar{n}$ pointing into the volume:

$$\iint\limits_{\partial V} (\Psi_2\nabla\Psi_1 - \Psi_1\nabla\Psi_2)\cdot\bar{n}\, dS = \iiint\limits_{V} \left(\Psi_1\nabla^2\Psi_2 - \Psi_2\nabla^2\Psi_1\right) dV. \tag{C.2}$$

Equation (C.2) is known as Green's second identity in which surface ∂V is piecewise continuous and the scalar functions Ψ_1 and Ψ_2 are assumed to be twice continuously differentiable.

Now, let us set for 3D flows

$$\Psi_1 = \frac{1}{r}, \qquad \Psi_2 = \Phi, \tag{C.3}$$

in which $\Phi(\vec{x}_P)$ is the velocity potential function in point $\vec{x}_P$ (see Figure C.1) and r is the distance from point $\vec{x}_Q$ on the enclosing surface to an arbitrary fixed point $\vec{x}_P$:

$$\vec{r} = \vec{x}_P - \vec{x}_Q, \quad r = |\vec{r}\,|, \qquad \text{where} \quad \vec{x}_Q \in \partial V. \tag{C.4}$$

Notice that

$$\nabla\frac{1}{r} = \frac{\vec{r}}{r^3}, \qquad \text{and} \qquad \nabla^2\frac{1}{r} = 0, \qquad \text{for} \qquad r \neq 0. \tag{C.5}$$

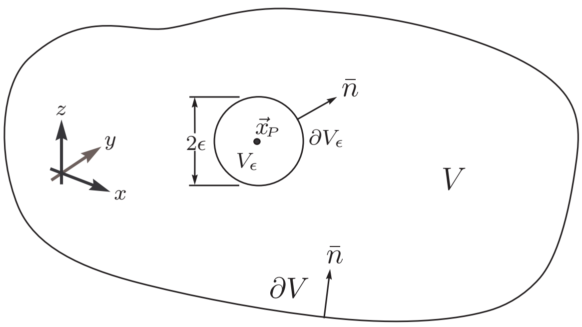

Figure C.1: Flow domain with region surrounding $\vec{x}_P \in V$ excluded from the domain of integration.

For point $\vec{x}_P$ outside flow domain V both Ψ_1 and Ψ_2 satisfy the Laplace equation and equation (C.2) becomes

$$\iint\limits_{\partial V} \left(\Phi \, \nabla \frac{1}{r} \; - \; \frac{1}{r} \nabla \Phi \right) \cdot \bar{n} \, dS \; = \; 0, \qquad \vec{x}_P \notin V. \tag{C.6}$$

In case point $\vec{x}_P$ is inside the domain of interest V, a small sphere with radius ϵ is introduced to exclude volume V_ϵ around point $\vec{x}_P$ from the volume of integration (see Figure C.1). Again, both Ψ_1 and Ψ_2 satisfy the Laplace equation and equation (C.2) now becomes

$$\iint\limits_{\partial V + \partial V_\epsilon} \left(\Phi \, \nabla \frac{1}{r} \; - \; \frac{1}{r} \nabla \Phi \right) \cdot \bar{n} \, dS \; = \; 0, \qquad \vec{x}_P \in V. \tag{C.7}$$

Now, let us evaluate the integral over the surface of the sphere ∂V_ϵ. With equation (C.5) we have

$$\iint\limits_{\partial V_\epsilon} \left(\Phi \, \nabla \frac{1}{r} \; - \; \frac{1}{r} \nabla \Phi \right) \cdot \bar{n} \, dS \; = \; \iint\limits_{\partial V_\epsilon} \left(\Phi \frac{\bar{n} \cdot \vec{r}}{r^3} \; - \; \frac{1}{r} \nabla \Phi \cdot \bar{n} \right) \, dS. \tag{C.8}$$

For a sphere with radius ϵ we have $\int dS = 4\pi\epsilon^2$. Assuming a continuously differentiable velocity potential Φ and letting $\epsilon \to 0$, the second term in equation (C.8) vanishes:

$$\iint\limits_{\partial V_\epsilon} \left(-\frac{1}{r} \nabla \Phi \cdot \bar{n} \right) \, dS \; = \; - \frac{\partial \Phi}{\partial n} \iint\limits_{\partial V_\epsilon} \left(\frac{1}{r} \right) \, dS \; = \; 0, \tag{C.9}$$

while for the first term in equation (C.8) we find

$$\iint\limits_{\partial V_\epsilon} \left(\Phi \frac{\bar{n} \cdot \vec{r}}{r^3} \right) \, dS \; = \; - \, \Phi(\vec{x}_P) \iint\limits_{\partial V_\epsilon} \left(\frac{1}{r^2} \right) \, dS \; = \; -4\pi \, \Phi(\vec{x}_P), \tag{C.10}$$

where we used for the normal vector on the sphere the expression

$$\bar{n} \; = \; \frac{\vec{x}_Q - \vec{x}_P}{|\vec{x}_Q - \vec{x}_P\,|} \; = \; -\frac{\vec{r}}{r}. \tag{C.11}$$

Substitution of this result in equation (C.7) gives an expression for the velocity potential Φ in an arbitrary point $\vec{x}_P \in V$ in terms of an integral over the boundaries ∂V:

$$\Phi(\vec{x}_P) \; = \; \frac{1}{4\pi} \iint\limits_{\partial V} \left(\Phi \, \nabla \frac{1}{r} \; - \; \frac{1}{r} \nabla \Phi \right) \cdot \bar{n} \, dS, \qquad \vec{x}_P \in V. \tag{C.12}$$

The same procedure can be followed for point $\vec{x}_P$ located on ∂V. Now only half a sphere is surrounding $\vec{x}_P$, assuming that $\vec{x}_P$ is not located at a surface-slope discontinuity. In addition, the intersection of the hemisphere with ∂V is excluded from the surface of integration (see Figure C.2). This results in the following integral:

$$\Phi(\vec{x}_P) \; = \; \frac{1}{2\pi} \iint\limits_{\partial V} \left(\Phi \, \nabla \frac{1}{r} \; - \; \frac{1}{r} \nabla \Phi \right) \cdot \bar{n} \, dS, \qquad \vec{x}_P \in \partial V. \tag{C.13}$$

In summary, we have found that

$$\frac{1}{4\pi} \iint\limits_{\partial V} \left(\Phi \, \nabla \frac{1}{r} \; - \; \frac{1}{r} \nabla \Phi \right) \cdot \bar{n} \, dS = \begin{cases} 0 & \vec{x}_P \notin V, \\ \frac{1}{2}\Phi(\vec{x}_P) & \vec{x}_P \in \partial V, \\ \Phi(\vec{x}_P) & \vec{x}_P \in V. \end{cases} \tag{C.14}$$

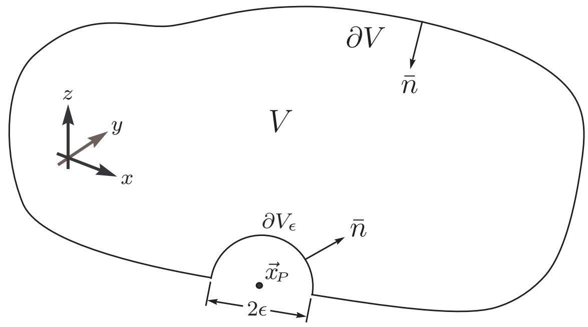

Figure C.2: Flow domain with region surrounding $\vec{x}_P \in \partial V$ excluded from the domain of integration.

Now, consider the situation in Figure C.3 in which we have a collection of non-overlapping subdomains V_m, each with a velocity potential function Φ_m. Some of the flow domains will have physical significance, while others are introduced to allow for certain boundary conditions, or for their influence on external regions. The boundary separating volume V_m from volume V_k is denoted by $S_{m,k}$

$$S_{m,k} = \partial V_m \cap \partial V_k, \qquad m \neq k, \tag{C.15}$$

and normal vector $\bar{n}_m$ is defined to point into subdomain V_m. The surface S of the configuration and its wake (see Figure C.3) are described by the complete set of inner boundaries:

$$S = \cup S_{m,k}. \tag{C.16}$$

The outer boundary $S_{0,1}$ is located either a finite or an infinite distance away from the inner boundaries in case of internal or external flows respectively.

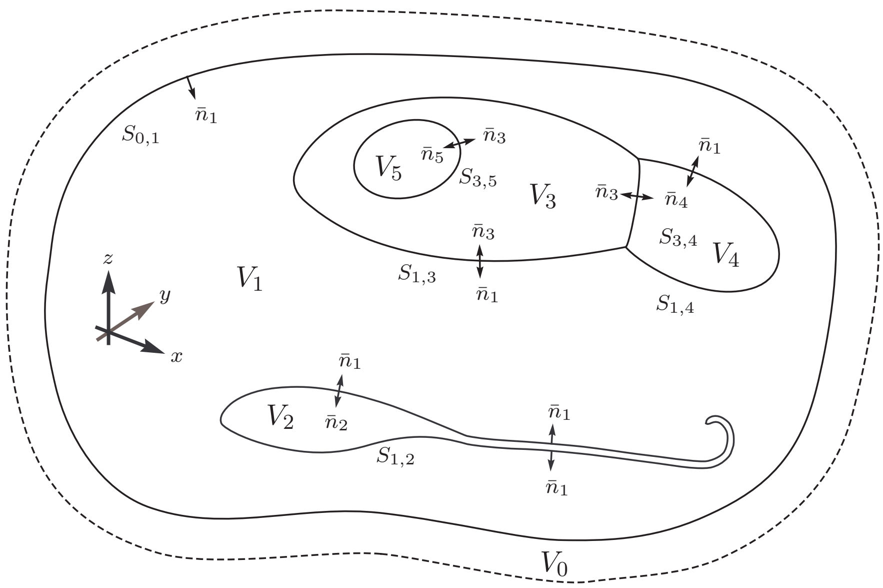

Figure C.3: Flow domain composed of non-overlapping volumes V_m and boundaries $S_{m,k}$ that separate volume V_m from volume V_k.

Summation of all surface integral contributions to the velocity potential in a point $\vec{x}_P \in V$ somewhere in the domain gives:

$$
\begin{aligned}
\Phi(\vec{x}_P) \;&=\; \frac{1}{4\pi}\iint\limits_{S}\left((\Phi_m-\Phi_k)\,\nabla\frac{1}{r}\;-\;\frac{1}{r}\nabla(\Phi_m-\Phi_k)\right)\cdot\bar{n}_m\;dS\;+\\
&\quad\frac{1}{4\pi}\iint\limits_{S_{0,1}}\left(\Phi_1\,\nabla\frac{1}{r}\;-\;\frac{1}{r}\nabla\Phi_1\right)\cdot\bar{n}_1\;dS,\qquad \vec{x}_P\in V.
\end{aligned}
\tag{C.17}
$$

If outer boundary $S_{0,1}$ lies an infinite distance away from the other boundaries, the contribution to $\Phi(\vec{x}_P)$ from the integral in equation (C.17) for $S_{0,1}$ can be considered to represent the unperturbed velocity potential $\Phi_\infty(\vec{x}_P)$ in the entire domain, i.e. the velocity potential if no inner boundaries were present. The integral contributions from the inner boundaries may thus be considered perturbation velocity potentials. Of course this is only valid if the velocity potential perturbation in equation (C.17) vanishes at infinity.

If we now define the dipole and source surface singularity strengths to be

$$
\mu = -\,(\Phi_m-\Phi_k,) \qquad \text{and} \qquad \sigma=\nabla(\Phi_m-\Phi_k)\cdot\bar{n}_m,
\tag{C.18}
$$

and, using the definition for $\vec{r}$ in equation (C.4), introduce the dipole and source perturbation velocity potentials

$$
\varphi_\mu(\vec{x}_P) \;=\; \frac{-1}{4\pi}\iint\limits_{S}\mu\,\frac{\bar{n}_m\cdot\vec{r}}{r^3}\;dS,
\tag{C.19}
$$

$$
\varphi_\sigma(\vec{x}_P) \;=\; \frac{-1}{4\pi}\iint\limits_{S}\sigma\,\frac{1}{r}\;dS,
\tag{C.20}
$$

we can reformulate boundary integral equation (C.17) as

$$
\Phi(\vec{x}_P)\;=\;\Phi_\infty(\vec{x}_P)\;+\;\varphi_\mu(\vec{x}_P)\;+\;\varphi_\sigma(\vec{x}_P),\qquad \vec{x}_P\in V.
\tag{C.21}
$$

The perturbation velocity potential functions as defined in equation (C.19) and equation (C.20) vanish towards infinity and satisfy the far-field condition mentioned. The integrals have a singular integrand which results in a jump in velocity potential across $S^\pm$ of size $-\mu$:

$$
\varphi(\vec{x}_P\to S^\pm)\;=\;\varphi^p_\sigma(\vec{x}_P\in S)+\varphi^p_\mu(\vec{x}_P\in S)\;\mp\;\frac{1}{2}\,\mu(\vec{x}_P\in S),
\tag{C.22}
$$

where S^+ and S^- denote the sides of $S_{m,k}$ when approached from volume V_m or from volume V_k respectively. The $\varphi^p(\vec{x}_P\in S)$ terms are to be interpreted as Cauchy principal value or Hadamard finite part integrals in which a small region around the singular point is excluded from the surface of integration.